Localized behavior in the Lyapunov vectors for quasi-one-dimensional many-hard-disk systems

Tooru Taniguchi and Gary P. Morriss
School of Physics, University of New South Wales, Sydney, New South Wales 2052, Australia
(Received 14 April 2003; published 13 October 2003)

We introduce a definition of a ''localization width'' whose logarithm is given by the entropy of the distribution of particle component amplitudes in the Lyapunov vector. Different types of localization widths are observed, for example, a minimum localization width where the components of only two particles are dominant. We can distinguish a delocalization associated with a random distribution of particle contributions, a delocalization associated with a uniform distribution, and a delocalization associated with a wavelike structure in the Lyapunov vector. Using the localization width we show that in quasi-one-dimensional systems of many hard disks there are two kinds of dependence of the localization width on the Lyapunov exponent index for the larger exponents: one is exponential and the other is linear. Differences due to these kinds of localizations also appear in the shapes of the localized peaks of the Lyapunov vectors, the Lyapunov spectra, and the angle between the spatial and momentum parts of the Lyapunov vectors. We show that the Krylov relation for the largest Lyapunov exponent $\lambda \sim -\rho \ln \rho$ as a function of the density ρ is satisfied (apart from a factor) in the same density region as the linear dependence of the localization widths is observed. It is also shown that there are asymmetries in the spatial and momentum parts of the Lyapunov vectors, as well as in their x and y components.

DOI: 10.1103/PhysRevE.68.046203 PACS number(s): 05.45.Jn, 05.45.Pq, 02.70.Ns, 05.20.Jj

I. INTRODUCTION

The dynamical instability of a system is essentially connected to the unpredictability of that system. It is described by the time evolution of the difference of two phase space vectors describing nearby trajectories, the so called Lyapunov vector. If the amplitude of the Lyapunov vector increases (decreases) rapidly in time, then the dynamics is unstable (stable) in the direction of the Lyapunov vector. An unstable orbit implies that a part of the dynamics is unpredictable and a statistical treatment may be required. The Lyapunov exponent, defined as the rate of exponential divergence or contraction of the amplitude of the Lyapunov vector with time, is the most frequently used indicator of the dynamical linear instability, and a system with a nonzero positive Lyapunov exponent is called chaotic. The Lyapunov exponent is connected to the transport coefficients, such as the conductance and viscosity [1]. In general, for each Lyapunov vector there is an individual Lyapunov exponent that is different in magnitude, and this leads to the concept of a sorted set of Lyapunov exponents, the so called Lyapunov spectrum.

Although the significance of the *amplitudes* of the Lyapunov vectors has been emphasized in the discussion of the dynamical instability, the Lyapunov vector itself including the information about its *angle* can play an important role in chaotic dynamics [1,2]. For example, the Lyapunov vector was used to characterize a high-dimensional chaotic attractor [3] and the clustered motion in symplectic coupled map systems [4]. One may also mention that the wavelike structure of the Lyapunov vectors associated with the stepwise structure of the Lyapunov spectra in the small (in absolute value) Lyapunov exponent region has been reported in many-hard-disk systems [5–8].

The localization of the Lyapunov vector for high-dimensional chaos, which we call the ''Lyapunov localization'' for convenience in this paper, is one of the chaotic behaviors which involves information on all the individual components of the Lyapunov vectors. The Lyapunov localization appears as the spatial localization of the largest components of the Lyapunov vector and is generally associated with the largest Lyapunov exponents. This phenomenon has been reported in the Kuramoto-Sivashinsky model [9], in coupled map lattice systems [10–12], in a random matrix model [13], in high-dimensional symplectic map systems [14], in many-hard-disk systems [15,16], etc. However it was not clear whether the Lyapunov localization has its origin in a randomness produced by the chaotic dynamics [17] (such as Anderson localization [18]) or if it comes simply from the short range property of particle interactions. For an understanding of Lyapunov localizations in coupled map lattice models and some nonlinear partial differential equations, a method using an analogy with the Kardar-Parisi-Zhang equation has been proposed [19,20], although this analogy is not universal as shown by some Hamiltonian systems such as nonharmonic oscillator chain models [21]. Moreover, the physical meaning and significances of this phenomenon is not well understood. One of the few suggestions about the importance of the Lyapunov localization is that it may be related to the existence of the thermodynamic limit for the largest Lyapunov exponent [15]. If the spatial localized region of the Lyapunov vector corresponding to the largest Lyapunov exponent is independent of the number of particles N in the thermodynamic limit, then the largest Lyapunov exponent can be N independent. This implies that the Kolmogorov-Sinai entropy, which is equal to the sum of all the positive Lyapunov exponents in closed systems, is an extensive quantity like the thermodynamic entropy. Besides, this gives some supporting evidence to the existence of the thermodynamic limit of the Lyapunov spectrum, which has been the subject of study in many-particle chaotic systems [9,22–24].

The principal aim of this paper is to use the Lyapunov localization as an indicator of the chaotic properties of many-particle systems. For quantitative considerations of the Lyapunov localization we use an entropylike quantity (or information dimension) of a distribution function of the amplitudes of the Lyapunov vector components for each particle [11,14]. We introduce the ''localization width'' as the quantity whose logarithm is given by this entropylike quantity. The value of the localization width is in the range $[1,N]$ and indicates the number of particles contributing to the localized part of the Lyapunov vector components. Using the localization width we can also distinguish different types of delocalized behaviors of the Lyapunov vectors, such as a delocalization associated with a random distribution of particle component amplitudes, a delocalization associated with a uniform distribution and a delocalization associated with a wavelike structure in the Lyapunov vector. As a concrete system to consider for the study of Lyapunov localization, we use a quasi-one-dimensional system consisting of many hard disks, in which the system shape is so narrow as to exclude the exchange of particle positions. In this system the minimum value of the localization width is given by 2, because particle interactions are given by collisions between *two* particles. In the quasi-one-dimensional systems each particle can interact only with its nearest-neighbor particles, so the numerical calculation is less time-consuming than for a fully two-dimensional hard-disk system in which each particle can collide with any other particle. The quasi-one-dimensional system also has the advantage that the roles of the coordinate directions are strongly separated. In our system the narrow direction (the y direction) of the rectangle is very much different from the longer orthogonal direction (the x direction). Another advantage of the use of the quasi-one-dimensional system is that there is a wider region of stepwise structure in the Lyapunov spectrum compared to a square two-dimensional system with the same number of particles and the same area [25]. This is a noticeable point because in this paper we show that the localization width is an indicator not only of the Lyapunov localization but also of the stepwise structure of the Lyapunov spectrum. Calculating the localization width in quasi-one-dimensional systems we show that there are two kinds of dependence of the Lyapunov index on the localization widths: an exponential dependence $[\mathcal{E}D]$ and a linear dependence $[\mathcal{L}D]$. (Here we define the Lyapunov spectrum as the set $\{\lambda^{(1)},\lambda^{(2)},\ldots,\lambda^{(4N)}\}$ of the Lyapunov exponents satisfying the condition $\lambda^{(1)}\geqslant\lambda^{(2)}\geqslant\cdots\geqslant\lambda^{(4N)}$ and introduce the Lyapunov index as the ordering number of the exponents in the Lyapunov spectrum.) The exponential dependence $[\mathcal{E}D]$ of the localization width appears at any particle density, and shows a tail in the spatial localized shape of the Lyapunov vector. On the other hand the linear dependence $[\mathcal{L}D]$ of the localization widths as a function of Lyapunov index appears only in cases of low particle density, and is characterized by a sharp rectangular localized shape of Lyapunov vector in space. Next, we consider the effects of the these two kinds of Lyapunov localizations on other quantities, such as the shape of the Lyapunov spectra, the angle between the spatial part and the momentum part of the Lyapunov vector, the amplitudes of the spatial part of the Lyapunov vector, etc. In particular, it is shown that apart from a prefactor the Krylov relation [41] for the largest Lyapunov exponent $\lambda\sim-\rho\ln\rho$ as a function of the particle density ρ is satisfied in the same density region in which the linear dependence $[\mathcal{L}D]$ of the localization widths appears. We also demonstrate a relation between localized regions of the Lyapunov vectors and the positions of colliding particles, suggesting that the Lyapunov localization comes from the short range interaction of the particles. We compare some of our results in quasi-one-dimensional systems with the square system with the same area and show that the two kinds of localizations appear in the square case as well.

As the second aim of this paper we investigate how the particle density and system shape affect the Lyapunov vector components. We show that the spatial part and the momentum part of the Lyapunov vectors are in almost the same direction at high density, whereas they are rather close to orthogonal in low density cases, especially in the region of the exponential dependence $[\mathcal{E}D]$ of the localization widths as a function of Lyapunov index. The amplitudes of the spatial part of the Lyapunov vectors are larger (smaller) than the corresponding momentum part in low (high) density cases. We also demonstrate that gaps appear in the amplitudes of the x and y components of both spatial and momentum parts of the Lyapunov vectors, because of the difference in roles of these directions in the quasi-one-dimensional system. In the amplitudes of the Lyapunov vector components we can also see effects due to the stepwise structure of the Lyapunov spectra.

The outline of this paper is as follows. In Sec. II we compare some quantities that characterize the Lyapunov localization and discuss the relative merits of the localization width comparing it with the other quantities. The relation between the localized region of Lyapunov vectors and the position of colliding particles is demonstrated. In Sec. III we show that there are two kinds of Lyapunov localizations. These two Lyapunov localizations are distinguished by their Lyapunov index dependences and the shapes of the localized peaks of the Lyapunov vectors. In Sec. IV we investigate the effects of the two kinds of Lyapunov localizations on the shape of the Lyapunov spectra and the angles and amplitudes of the Lyapunov vectors components, etc. The Lyapunov index dependence of the x and y components of the spatial part and the momentum part of the Lyapunov vectors are shown. In Sec. V we investigate the density dependences of quantities associated with the largest Lyapunov exponent such as the largest Lyapunov exponent itself, the angle of the Lyapunov vectors and the localization width, etc., and specify the density region in which the linear dependence $[\mathcal{L}D]$ of the localization width on Lyapunov index appears. The region of Lyapunov indices, in which the linear dependence $[\mathcal{L}D]$ of the Lyapunov widths appears, is connected to the region in which the Krylov relation for the density dependence of the largest Lyapunov exponent is satisfied. Section VI is our conclusions and further remarks. In Appendix A we give a derivation of an inequality for the localization width. In Appendix B we compare some results for the quasi-

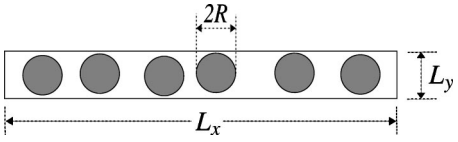

FIG. 1. The quasi-one-dimensional system that we consider. The system shape is so narrow that the particles always remain in the same order.

one-dimensional systems in the text with those of corresponding square systems.

II. LOCALIZATION WIDTH OF LYAPUNOV VECTORS

We consider the quasi-one-dimensional system that consists of N hard-disks with radius R. The shape of the system is a two-dimensional rectangle satisfying the condition

$$RN\sqrt{3}<L_x \quad \text{and} \quad 2R<L_y<4R, \tag{1}$$

with width L_x and height L_y. Condition (1) means that the system is so narrow that the positions of particles cannot be exchanged. The systems satisfying this condition are referred to as quasi-one-dimensional systems in this paper. The schematic illustration of such a system is given in Fig. 1. The quasi-one-dimensional system was used to discuss the stepwise structure of the Lyapunov spectra and the associated wavelike structure of the Lyapunov vectors in Ref. [25].

In this paper we consider the case where the parameter values are given by the radius of particles, $R=1$; the mass of particles, $M=1$; and the total energy of system, $E=N$. The system size is given by $L_y=2R(1+10^{-6})$ and $L_x=NL_y(1+d)$ satisfying condition (1) with a constant d (except in Appendix B where we consider square systems.) Roughly speaking, the factor $1+d$ is the averaged ratio of the distances that each particle can move in the x direction and the y direction. The constant d is connected to the density

$$\rho \equiv \frac{N\pi R^2}{L_x L_y} = \frac{\pi R^2}{(1+d)L_y^2} \tag{2}$$

as $d=\pi R^2/(\rho L_y^2)-1$ [26].

The quasi-one-dimensional many-hard-disk system has many advantages for numerical investigations of the dynamical properties of many-particle systems. First, in many-hard-disk systems the free flight part of the dynamics is integrable, so the actual numerical calculations of phase space dynamics and tangent space dynamics are simply described by multiplications of the time-evolutional matrices corresponding to free flight and collision. Second, in the quasi-one-dimensional system defined by Eq. (1) each particle can only collide with its two nearest-neighbor particles, so we do not need to search every particle pair to find the colliding pair. These points lead to a faster numerical calculation of the dynamical properties (especially Lyapunov spectra and Lyapunov vectors) than for other many-particle systems, such as fully two-dimensional particle systems (in which any pair of particles can collide) or with particles with soft-core interactions. Another advantage of the quasi-one-dimensional system is that the roles of the x and y directions are separated, so we can investigate how such a separated role for the directions affects, for example, the Lyapunov exponents and Lyapunov vectors. In the quasi-one-dimensional system the particle positions are roughly equivalent to the particle indices, so we can discuss the dynamics of quantities using three-dimensional graphs as functions of the collision number and particle index, which is much simpler than the full of two-dimensional system that requires four-dimensional graphs as functions of the time, the x and y components of particle positions. Finally in quasi-one-dimensional many-hard-disks, we get a wider stepwise region of the Lyapunov spectra rather than in the fully two-dimensional square systems. This was an essential point in the study of the stepwise structure of Lyapunov spectra and the associated wavelike structure of the Lyapunov vectors in systems with small numbers of particles in Ref. [25].

We introduce the Lyapunov vector as $\delta\mathbf{\Gamma}^{(n)}(t) \equiv (\delta\mathbf{\Gamma}_1^{(n)}(t), \delta\mathbf{\Gamma}_2^{(n)}(t), \ldots, \delta\mathbf{\Gamma}_N^{(n)}(t))$ corresponding to the n-th Lyapunov exponents $\lambda^{(n)}$ at time t. Here, $\delta\mathbf{\Gamma}_j^{(n)}(t)$ is the Lyapunov vector component corresponding to the jth particle and the Lyapunov exponent $\lambda^{(n)}$ at time t. We define the normalized amplitude $\gamma_j^{(n)}(t)$ of the Lyapunov vector components $\delta\mathbf{\Gamma}_j^{(n)}(t)$ by

$$\gamma_j^{(n)}(t) \equiv \frac{|\delta\mathbf{\Gamma}_j^{(n)}(t)|^2}{\sum_{k=1}^{N} |\delta\mathbf{\Gamma}_k^{(n)}(t)|^2}, \tag{3}$$

so that the conditions

$$\sum_{j=1}^{N} \gamma_j^{(n)}(t) = 1, \tag{4}$$

$$0 \leqslant \gamma_j^{(n)}(t) \leqslant 1 \tag{5}$$

are automatically satisfied. Figures 2(a) and 2(b) are two typical behaviors of the Lyapunov vector components for the largest Lyapunov exponent as functions of the collision number n_t and the particle index j for (a) $d=1.5$ (or density $\rho=0.314\ldots$) and (b) $d=10^5$ (or density $\rho=0.000\,007\,85\ldots$). Here we take the particle index j so that the x-component $q_{xj}(t)$ of the jth particle satisfies the condition $q_{x1}(t_0)<q_{x2}(t_0)<\cdots<q_{xN}(t_0)$ at the initial time $t=t_0$ and the data are taken every two collisions. (It should be noted that the collision number n_t is related to the time t approximately by multiplying by the mean free time, and in the quasi-one-dimensional system the particle index j has a similar meaning to the x component of the particle position.) These graphs show clearly that a nonzero value of the quantity $\gamma_j^{(1)}(t)$ is localized in a small spatial region involving a few particles. Localized peak positions stay in almost the same position over several tens of collisions, then seem to hop to another position. Details of the localized behaviors of the quantity $\gamma_j^{(1)}(t)$, especially the differences between Figs. 2(a) and 2(b), will be discussed in the following sections and are the main purpose of this paper.

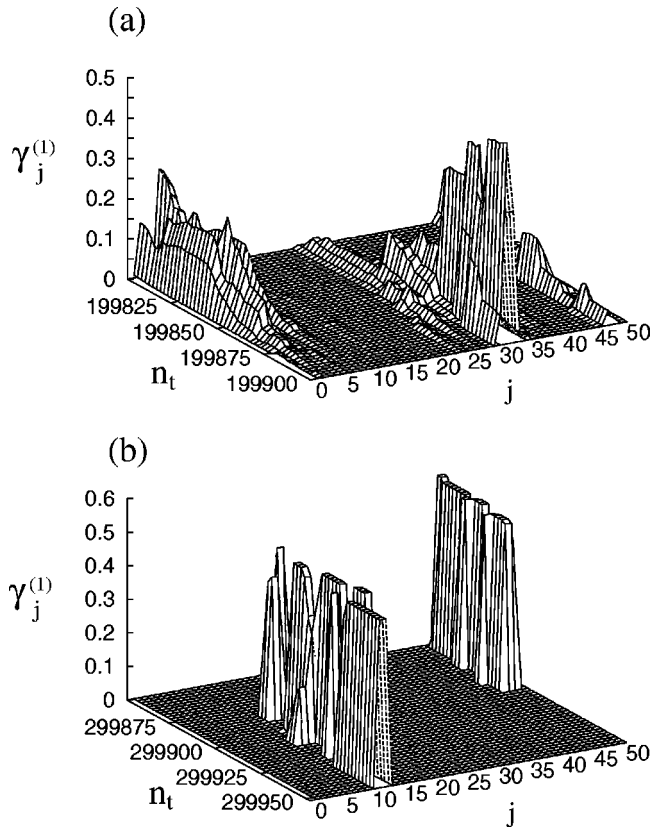

FIG. 2. Localized behaviors of the amplitudes $\gamma_j^{(1)}$ of the normalized Lyapunov vector components of the jth particle corresponding to the largest Lyapunov exponent $\lambda^{(1)}$ as functions of the collision number n_t and the particle index j in a quasi-one-dimensional system of $N=50$ for (a) high density $d=1.5$ and (b) low density $d=10^5$.

To obtain our numerical results we use the algorithm developed by Benettin *et al.* [27] and Shimada and Nagashima [28]. This algorithm is characterized by intermittent reorthogonalization and renormalization of Lyapunov vectors, which can be done after each particle collision in a many-hard-disk system. Other papers such as Refs. [29–31] should be referred to for more details of this algorithm and the Lyapunov vector dynamics of many-hard-disk systems.

Now we discuss methods to characterize the strength of the localization of the Lyapunov vectors as those in Figs. 2(a) and 2(b) in a quantitative sense. By analogy to the localization length used in Anderson localization [18] it may be suggested that the strength of the Lyapunov localization can be characterized by a localization length $\Omega^{(n)}$ defined by

$$[\Omega^{(n)}]^{-1} \equiv \lim_{j\to\infty} \lim_{N\to\infty} j^{-1} \langle \ln \gamma_j^{(n)}(t) \rangle \tag{6}$$

as the number of particles N goes to infinity, namely, in the thermodynamic limit. Here we use the bracket $\langle \mathcal{X} \rangle$ to signify the long time average of the time-dependent quantity $\mathcal{X}$. [Note that in definition (6) of the localization length $\Omega^{(n)}$ we used the fact that the system is quasi-one-dimensional. In more general cases, such as a fully two-dimensional system, the limit $j\to\infty$ in Eq. (6) must be replaced by the limit of the amplitude of the spatial coordinate.] This quantity $\Omega^{(n)}$ characterizes the Lyapunov localization as its spatial exponential decay rate. However this quantity may not be suitable to characterize the localization as that in Fig. 2(b) which does not have an exponential decay. Besides, this quantity requires the thermodynamic limit $N\to\infty$. The numerical calculation of the Lyapunov spectrum and Lyapunov vectors for many-particle systems is very time-consuming and has so far only been reported for systems of about 1000 particles [16], so it may be rather difficult to estimate the quantity $\Omega^{(n)}$ defined by Eq. (6) numerically.

Another method to characterize the Lyapunov localization was proposed in Ref. [15]. In this method we first introduce a parameter threshold $\Theta \in (0,1)$ and define the quantity $C_\Theta^{(n)}$ as

$$C_\Theta^{(n)} \equiv \min_x \left\{ x; \Theta < \sum_{j=1}^{Nx} \langle \tilde{\gamma}_j^{(n)}(t) \rangle \right\} \tag{7}$$

with an integer Nx and the sorted set

$$\{\tilde{\gamma}_1^{(n)}(t), \tilde{\gamma}_2^{(n)}(t), \ldots, \tilde{\gamma}_N^{(n)}(t)\} = \{\gamma_1^{(n)}(t), \gamma_2^{(n)}(t), \ldots, \gamma_N^{(n)}(t)\}$$

satisfying the condition $\tilde{\gamma}_1^{(n)}(t) \geqslant \tilde{\gamma}_2^{(n)}(t) \geqslant \cdots \geqslant \tilde{\gamma}_N^{(n)}(t)$. This quantity $C_\Theta^{(n)}$ is a measure of the number of particle components actively contributing to a localized part of the Lyapunov vector for the nth Lyapunov exponent $\lambda^{(n)}$. This quantity $C_\Theta^{(n)}$ does not require the thermodynamic limit, and can be suitable for both types of the Lyapunov localizations shown in Fig. 2. However this quantity is a function of an artificial threshold Θ, which cannot be determined by the dynamics itself.

In this paper we discuss the Lyapunov localization by using an entropylike quantity for the amplitude distribution $\gamma_j^{(n)}(t)$ of the normalized Lyapunov vector elements, namely, the entropylike quantity $S^{(n)}$ defined by

$$S^{(n)} \equiv -\sum_{j=1}^{N} \langle \gamma_j^{(n)}(t) \ln \gamma_j^{(n)}(t) \rangle, \tag{8}$$

noting that the quantity $\gamma_j^{(n)}(t)$ satisfies conditions (4) and (5) so it can be regarded as a kind of distribution function. Using this quantity $S^{(n)}$ we introduce the quantity $\mathcal{W}^{(n)}$ as

$$\mathcal{W}^{(n)} \equiv \exp\{S^{(n)}\}, \tag{9}$$

which we call the nth "localization width" corresponding to the nth Lyapunov exponent $\lambda^{(n)}$. This localization width has already been used to discuss the Lyapunov localization in a coupled map lattice model [11] and a high-dimensional symplectic map system [14].

To understand the physical meaning of the localization width $\mathcal{W}^{(n)}$ defined by Eq. (9) it is useful to discuss some of its properties. The first property of the localization width is the inequality

$$1 \leqslant \mathcal{W}^{(n)} \leqslant N. \tag{10}$$

The derivation of inequality (10) is given in Appendix A. The second property of the localization width $\mathcal{W}^{(n)}$ is that the equality $\mathcal{W}^{(n)}=1$ is satisfied only when one of the quantities $\gamma_j^{(n)}(t)$, $j=1,2,\ldots,N$ is equal to 1, namely, in the most localized case, and the equality $\mathcal{W}^{(n)}=N$ is satisfied only when all of these quantities are equal to each other, namely, $\gamma_1^{(n)}(t)=\gamma_2^{(n)}(t)=\cdots=\gamma_N^{(n)}(t)=1/N$, namely, in the most delocalized case (see Appendix A about this point). These properties suggest that the localization width $\mathcal{W}^{(n)}$ also indicates the number of particles contributing to the localized part of the Lyapunov vector, which is analogous to the quantity $NC_\Theta^{(n)}$ derived from Eq. (7). The third property of the localization width comes from the symplectic structure of the Hamiltonian dynamics. To discuss this property we note the conjugate relation [1]

$$\delta\mathbf{\Gamma}_j^{(4N-n+1)}\equiv\begin{pmatrix}\delta\mathbf{q}_j^{(4N-n+1)}\\ \delta\mathbf{p}_j^{(4N-n+1)}\end{pmatrix}=\xi^{(n)}\begin{pmatrix}\delta\mathbf{p}_j^{(n)}\\ -\delta\mathbf{q}_j^{(n)}\end{pmatrix} \tag{11}$$

for the Lyapunov vector component $\delta\mathbf{\Gamma}_j^{(4N-n+1)}$ of the jth particle corresponding to the $(4N-n+1)$th Lyapunov exponent

$$\lambda^{(4N-n+1)}=-\lambda^{(n)}, \tag{12}$$

$n=1,2,\ldots,2N$, where $\delta\mathbf{q}_j^{(n)}$ and $\delta\mathbf{p}_j^{(n)}$ are the spatial part and the momentum part of the Lyapunov vector $\delta\mathbf{\Gamma}_j^{(n)}$ of the jth particle, respectively, and $\xi^{(n)}$ is a constant depending on the Lyapunov index only. [As a remark, if we use the Benettin algorithm to calculate the Lyapunov spectra, which is characterized by the intermittent normalization (as well as the reorthogonalization of Lyapunov vectors, the factor $\xi^{(n)}$ in Eq. (11) is given by $+1$ or -1 depending on the Lyapunov index n.] From Eqs. (3) and (11) we derive

$$\gamma_j^{(4N-n+1)}(t)=\gamma_j^{(n)}(t) \tag{13}$$

at any time t, where j is the particle index and $n=1,2,\ldots,2N$ is the Lyapunov index. Equations (8), (9), and (13) lead to the third property of the localization width

$$\mathcal{W}^{(4N-n+1)}=\mathcal{W}^{(n)}. \tag{14}$$

This is the conjugate property for the localization width $\mathcal{W}^{(n)}$.

Some of the advantages and disadvantages of the use of the localization width $\mathcal{W}^{(n)}$ to discuss the Lyapunov localizations are as follows. An advantage of the localization width $\mathcal{W}^{(n)}$ is that its calculation does not require the thermodynamic limit, different from the localization length $\Omega^{(n)}$ defined by Eq. (6). Besides, the localization width $\mathcal{W}^{(n)}$ is applicable to the Lyapunov localization seen in Fig. 2(b), whereas the localization length $\Omega^{(n)}$ requires that the tail of the quantity $\gamma_j^{(n)}(t)$ decay exponentially in space. Moreover the localization width $\mathcal{W}^{(n)}$ does not require an artificial parameter such as the threshold $\Theta\in(0,1)$ in the quantity $C_\Theta^{(n)}$ defined by Eq. (7), so it can be determined from the dynamics only. On the other hand, a disadvantage of the localization width $\mathcal{W}^{(n)}$ is that using this quantity, for example, we cannot distinguish between *one* peak of height α and width 2β with constants α and β and *two* peaks of height α and width β which should be recognized as different localized behaviors. Therefore, in principle we have to look at the concrete shapes of localized peaks to check the relation between this localization width and the peak width in actual numerical calculations, even if we calculate the localization width of the Lyapunov vector. The quantity $C_\Theta^{(n)}$ defined by Eq. (7) also has the same disadvantage.

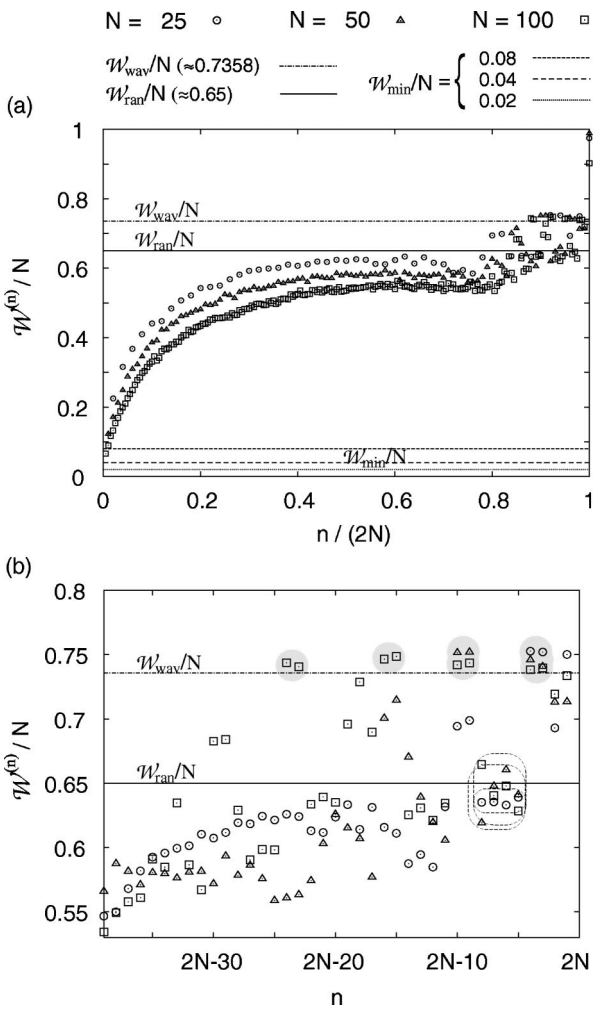

FIG. 3. Normalized localization widths $\mathcal{W}^{(n)}/N$ in the case of $d=0.5$. The circles, triangles, and squares correspond to the cases of $N=25$, 50, and 100, respectively. The dash-dotted line, solid line, and dashed lines (and the dotted line) correspond to $\mathcal{W}^{(n)}=\mathcal{W}_{wav}$ ($\approx 0.736N$), $\mathcal{W}_{ran}$ ($\approx 0.651N$) and $\mathcal{W}_{min}$ ($=2$), respectively. (a) Full scale of the normalized localization widths as functions of the normalized Lyapunov index $n/(2N)$. (b) An enlarged graph of the normalized localization widths corresponding to the small positive Lyapunov exponent region as functions of the Lyapunov index n. Symbols with a gray-filled background correspond to the two-point steps of the Lyapunov spectra which are indicated by similar circles in Fig. 4. Symbols surrounded by a rectangle of dashed lines correspond to the four-point steps of the Lyapunov spectra which are indicated by similar rectangles surrounding symbols in Fig. 4.

Figure 3 are examples of graphs of localization widths as

functions of the Lyapunov index in quasi-one-dimensional systems. We have plotted the normalized localization widths $\mathcal{W}^{(n)}/N$ for different system sizes for quasi-one-dimensional systems where $d=0.5$ (density $\rho=0.523\ldots$). In order to take the time average in Eq. (8) to calculate the localization width, we sample the quantities $\gamma_j^{(n)}(t)\ln\gamma_j^{(n)}(t)$ just after collisions for $1000N$ collisions and take the arithmetic average. (In this paper we always calculate localization widths in this way.) Figure 3(a) is the full scale graph of the localization widths as functions of the normalized Lyapunov index $n/(2N)$, and Fig. 3(b) shows a part of the localization widths corresponding to the small positive Lyapunov exponent region as functions of the Lyapunov index n. [Note that we use the normalized Lyapunov index $n/(2N)$ for the x axis in Fig. 3(a), which is different from the x axis as the Lyapunov index n itself in Fig. 3(b).] The plot of the values of the localization widths $\mathcal{W}^{(n)}$, $j=2N+1,2N+2,\ldots,4N$ is omitted because of the conjugate relation (14). In the region of large positive Lyapunov exponents the localization width $\mathcal{W}^{(n)}$ is a monotonically increasing function of the Lyapunov index n. This implies that localized behavior of the Lyapunov vector is stronger in the large (in absolute value) Lyapunov exponent region. The shape of the localization width in this region is similar qualitatively to the shape given by the quantity $C_\Theta^{(n)}$ defined by Eq. (7) which was calculated in a square system [16]. Figure 3(a) also shows that the value of the normalized Lyapunov localization widths $\mathcal{W}^{(n)}/N$ decreases as a function of particle number N in the region where Lyapunov spectra change smoothly. Noting that the localization width has a lower bound ($\mathcal{W}^{(n)}/N\geqslant 1/N$), this suggests the existence of the thermodynamic limit for the spectrum of the localization widths.

Another important point in Fig. 3 is the connection with the stepwise structure of Lyapunov spectra. Figure 4 shows the normalized Lyapunov spectra as a function of the Lyapunov index n for different system sizes for $d=0.5$. These three system sizes correspond to those of Fig. 3 for the localization width. In this figure the stepwise structures of Lyapunov spectra appear in the small Lyapunov exponent region. The values of the largest Lyapunov exponents are $\lambda^{(1)}\approx 1.28$ for $N=25$, $\lambda^{(1)}\approx 1.31$ for $N=50$, $\lambda^{(1)}\approx 1.31$ for $N=100$. The inset to Fig. 4 shows the full scale graph of the positive branch of the Lyapunov spectra normalized by the largest Lyapunov exponents as functions of the normalized Lyapunov index $n/(2N)$ (note again that we use the different horizontal axes in the main graphs and the inset into Fig. 4), and show that the global shapes of these graphs are similar and almost independent of the particle number N except in the small exponent region. Comparing Fig. 4 with Fig. 3(b) for the localization widths in the same region of the Lyapunov index n, we notice that the localization widths $\mathcal{W}^{(n)}/N$ normalized by the particle number N corresponding to the clear two-point steps of the Lyapunov spectra take almost same value, which is almost independent of the sequence of the steps and the particle number N [see the symbols with a gray-filled background in Figs. 3(b) and 4 about this point]. A similar thing can be seen for the four-point steps of the Lyapunov spectra. [See the symbols surrounded by a rectangle of dashed lines in Figs. 3(b) and 4.] One may

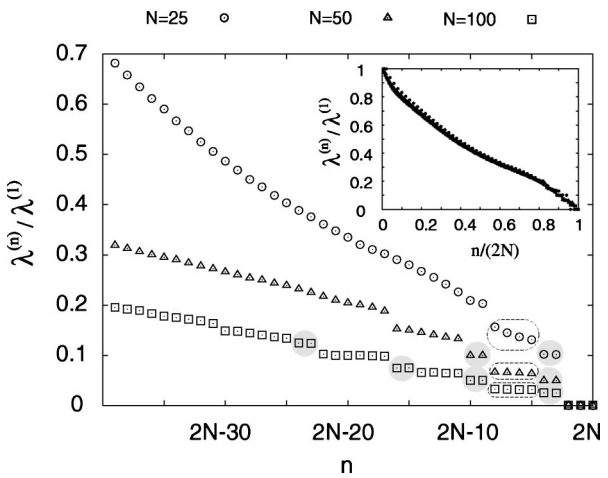

FIG. 4. Lyapunov spectra normalized by the largest Lyapunov exponent $\lambda^{(1)}$ as a function of the Lyapunov index n for $d=0.5$. The circles, triangles, and squares correspond to the cases of $N=25$,50, and 100, respectively. Symbols with a gray-filled background correspond to symbols with similar circles in Fig. 3(b). Symbols surrounded by a rectangle of dashed lines correspond to symbols surrounded by similar rectangles in Fig. 3(b). Inset: The full scale graph of the positive branch of the Lyapunov spectra as functions of the normalized Lyapunov index $n/(2N)$ for $N=25$,50, and 100. Notice that their global shapes are almost indistinguishable everywhere except in the small exponent region.

also notice that the region of the localization widths corresponding to the stepwise region of the Lyapunov spectra, which is around the region $n/(2N)>0.8$ of the Lyapunov index n in Fig. 3 approximately, can be distinguished from the other region. These points about the localization widths that connect with the stepwise structure of the Lyapunov spectra are other merits of the use of the localization width to discuss the behavior of the Lyapunov vectors.

Before finishing this section, it is valuable to summarize some specific values of the localization width $\mathcal{W}^{(n)}$ which have a clear physical meaning. The first value of the localization width is $\mathcal{W}^{(n)}=\mathcal{W}_{max}\equiv N$ in which the amplitudes $|\delta\mathbf{\Gamma}_j^{(n)}|$ of the Lyapunov vector components for each particle take the same value. The Lyapunov localization close to this value actually occurs in one of the zero-Lyapunov exponents, as shown in $\mathcal{W}^{(2N)}/N$ in Fig. 3(a). The second value is a lower bound for the Lyapunov localization: $\mathcal{W}^{(n)}\geqslant\mathcal{W}_{min}\equiv 2$. This is a little stronger condition than the inequality $\mathcal{W}^{(n)}\geqslant 1$ which we have already shown in the inequality (10). This value of the localization width is shown in Fig. 3 as the dotted line (the three lines of $\mathcal{W}^{(n)}/N=2/N=0.08$ for $N=25$, $2/N=0.04$ for $N=50$, and $2/N=0.02$ for $N=100$). This lower bound for the localization width comes from the fact that particle collisions occur between *two* particles, and is partly supported by the fact that the width of the amplitudes $\gamma_j^{(n)}$ of the normalized Lyapunov vector components of the jth particle corresponding to the nth Lyapunov exponent $\lambda^{(n)}$ is almost 2 in the low density limit and in large Lyapunov exponents, for example, as shown in Fig. 2(b). It should also be emphasized that there is a relation between the localized region of a Lyapunov vector and positions of

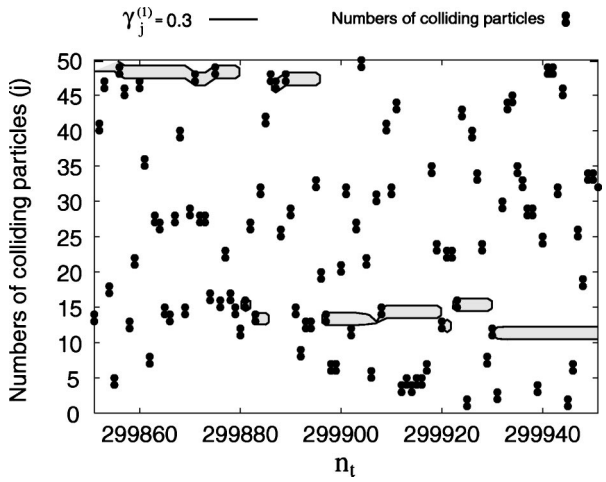

FIG. 5. Localized regions (gray-filled and surrounded by solid lines) of the Lyapunov vector $\delta\mathbf{\Gamma}^{(1)}$ and the numbers of colliding particle pairs (as pairs of black-filled circles) as functions of the collision number n_t and particle number j in a quasi-one-dimensional system of $N=50$ and $d=10^5$. The solid line is the contour plot $\gamma_j^{(1)}=0.3$ of the amplitudes of the normalized Lyapunov vector components $\gamma_j^{(1)}$ of the jth particle corresponding to the largest Lyapunov exponent $\lambda^{(1)}$, for the state shown in Fig. 2(b).

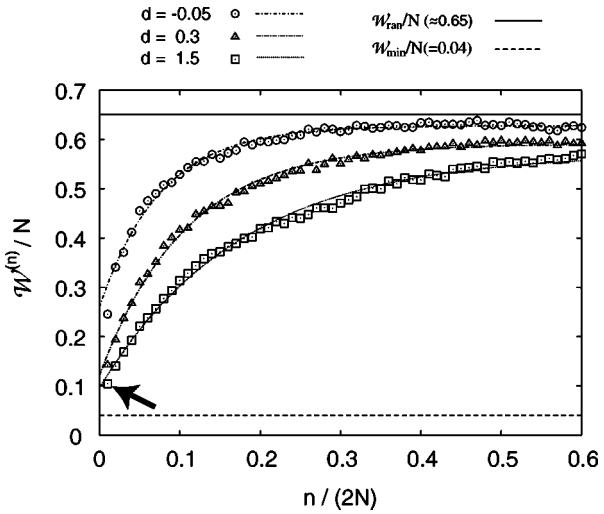

FIG. 6. Normalized localization widths $\mathcal{W}^{(n)}/N$ as functions of the normalized Lyapunov index $n/(2N)$ in high density cases of $d=-0.05$ (circles), $d=0.3$ (triangles) and $d=1.5$ (squares). The data are fitted by exponential functions. The localization widths $\mathcal{W}^{(n)}=\mathcal{W}_{ran}$ and $\mathcal{W}_{min}$ are indicated by the solid line and the dashed line, respectively. The localization width indicated by the arrow corresponds to the localized behavior of the Lyapunov vector shown in Fig. 2(a).

colliding particle pairs. To show this, in Fig. 5 we plot colliding particle pairs as well as a contour plot of the amplitude $\gamma_j^{(1)}$ as a function of the collision number n_t and the particle number j for the quasi-one-dimensional system with $N=50$ and $d=10^5$, which correspond to the three-dimensional plot of the Lyapunov localization given in Fig. 2(b). It is clear from this figure that particle collisions occur at the beginning of the sharp rectangular shapes of the localization of the amplitudes $\gamma_j^{(n)}$. This suggests that the Lyapunov localization comes from the short range of particle-particle interactions. The minimum value of the localization width will also be discussed in Secs. III B and V C in this paper. The third value of the localization width is the value for the case in which the amplitudes $\gamma_j^{(n)}(t)$, $k=1,2,\ldots,N$ are distributed randomly with an equal probability (the solid line in Fig. 3). It is given by $\mathcal{W}^{(n)}=\mathcal{W}_{ran}\approx 0.651N$ approximately, and gives an upper bound on the localization widths for Lyapunov indices corresponding to the continuous part of the Lyapunov spectrum [32]. The fourth value of the localization width is the value obtained for a wavelike structure in the Lyapunov vector. The dashed line in Fig. 3 is given as the localization width of $\gamma_j^{(n)}(t)=|\alpha_j^{(n)}(t)\sin[2\pi jn/N+\beta(t)]|^2$, where the constant $\alpha_j^{(n)}(t)$ is determined by the normalization condition for $\gamma_j^{(n)}(t)$ and $\beta(t)$ is randomly chosen from a uniform distribution in $[0,2\pi)$. Our numerical estimate for the localization width $\mathcal{W}^{(n)}$ in such a case is n independent and is given approximately by $\mathcal{W}^{(n)}=\mathcal{W}_{wav}\approx 0.736N$. Figure 3(b) shows that some of the localization widths are in this range (the dash-dotted line), and they correspond to the transverse Lyapunov mode, namely, a wavelike structure in the Lyapunov vectors corresponding to the two-point steps of the Lyapunov spectrum [5,25].

III. DENSITY DEPENDENCE OF THE LYAPUNOV LOCALIZATION

In this section we compare the Lyapunov localization widths $\mathcal{W}^{(n)}$ as a function of the Lyapunov index at different densities. We concentrate on the region where the Lyapunov spectra change smoothly as a function of the Lyapunov index and show that there are two kinds of Lyapunov index dependence of the localization widths: exponential dependence $[\mathcal{E}D]$ and linear dependence $[\mathcal{L}D]$. In the remaining sections of this paper the number of particle is $N=50$, and we change the particle density ρ by changing the parameter d connected to ρ by Eq. (2).

A. Lyapunov localization at high density

Figure 6 shows the normalized Lyapunov localization widths as functions of the normalized Lyapunov index $n/(2N)$ for a range of densities. In this figure the random component localization width $\mathcal{W}_{ran}\approx 0.65N$ and the minimum localization width $\mathcal{W}_{min}=2$ are indicated by the solid line and the dashed line, respectively. We fitted the graphs to exponential functions $y=\alpha_d+\beta_d\exp(\gamma_d x)$ with fitting parameters α_d, β_d, and γ_d. Here we find the best values of the fitting parameters to be $(\alpha_{-0.05},\beta_{-0.05},\gamma_{-0.05})=(0.627\,454,-0.366\,969,-13.1761)$, $(\alpha_{0.3},\beta_{0.3},\gamma_{0.3})=(0.590\,977,-0.469\,104,-9.334\,07)$ and $(\alpha_{1.5},\beta_{1.5},\gamma_{1.5})=(0.572\,315,-0.476\,522,-5.700\,97)$. The localization widths $\mathcal{W}^{(n)}$ are nicely fitted by these exponential functions in the region $n/(2N)\leqslant 0.6$ (the exponential dependence region $[\mathcal{E}D]$).

Figure 6 also shows that the localization widths decrease as the parameter d increases (therefore as the density ρ decreases). The largest Lyapunov exponent is an increasing

function of the particle density, as will be discussed in Sec. V, so this result means that the Lyapunov localization is stronger in a system with weaker chaos as characterized by a smaller value of the largest Lyapunov exponent. It should also be noted that in this region the localization widths are smaller than the random localization width $\mathcal{W}_{ran} \approx 0.65N$, and larger than $\mathcal{W}_{min} = 2$. Figure 2(a) shows the behavior of the Lyapunov localization corresponding to the localization width indicated by the arrow in Fig. 6. It is important to note that the shape of the quantities $\gamma_j^{(n)}(t)$ as a function of the particle index j have a tail like that in Fig. 2(a) in the region showing an exponential dependence $[\mathcal{E}D]$ of the localization widths.

B. Lyapunov localization at low density

Now we consider the Lyapunov localization in low density cases, given by large values of the parameter d. Figure 7(a) shows the normalized localization widths $\mathcal{W}^{(n)}/N$ as functions of the normalized Lyapunov index $n/(2N)$ for various values of d for the region where the Lyapunov spectra change smoothly. It is clear that the Lyapunov index dependences of the localization widths in this figure are different from the high density cases shown in Fig. 6 in a number of senses. First, linear dependences of the localization widths with respect to the Lyapunov index appear in the region of small localization widths, which correspond to the larger Lyapunov exponents. In Fig. 7(b), fits of the Lyapunov index dependences of the localization widths by linear functions $y = \tilde{\alpha}_d x + \tilde{\beta}_d$ are given with fitting parameters $\tilde{\alpha}_d$ and $\tilde{\beta}_d$: $(\tilde{\alpha}_{10^2}, \tilde{\beta}_{10^2}) = (0.503\,874, 0.046\,405)$ in the case of $d = 10^2$, $(\tilde{\alpha}_{5\times10^2}, \tilde{\beta}_{5\times10^2}) = (0.347\,437, 0.044\,468)$ in the case of $d = 5\times10^2$, and $(\tilde{\alpha}_{10^5}, \tilde{\beta}_{10^5}) = (0.224\,129, 0.042\,750\,6)$ in the case of $d = 10^5$. It is important to note that the localization widths are always larger than 2, namely, $\mathcal{W}^{(n)}/N > 2/N = 0.04$ in this figure, and the smallest localization widths corresponding to the largest Lyapunov exponents are close to this minimum value in these low density cases. Besides, the graph of the linear dependence of the localization widths is flatter in the lower density case, as shown by the fact that the value of the fitting parameter $\tilde{\alpha}_d$ decreases as the value of the parameter d increases. The existence of the linear dependence $[\mathcal{L}D]$ of the localization widths is one of the main results of this paper. (In Fig. 7(a) the region of the linear dependence $[\mathcal{L}D]$ in the low density limit is shaded gray.) Second, in Fig. 7(a) we can still recognize a region of localization widths in which the Lyapunov index dependence of the Lyapunov localization widths is exponential (the exponential dependence $[\mathcal{E}D]$ region). To show it clearly we give a fit of an exponential function $y = \alpha' + \beta' \exp(\gamma' x)$ with values $(\alpha', \beta', \gamma') = (0.560\,814, -2.733\,48, -7.505\,43)$ of the fitting parameters in Fig. 7(a). It should be emphasized that the shapes of the localization widths in the $[\mathcal{E}D]$ region are almost independent of the particle density ρ, at least in the three density cases shown in Fig. 7(a). As the third point, one may notice that from the above characteristics of the localization widths in the low density cases the region of the linear dependence $[\mathcal{L}D]$ and the region of the exponential dependence $[\mathcal{E}D]$ are more distinguishable in the lower density case, with an accompanying sharp bending of the localization width profile. Figure 7 suggests that the spectrum of the localization widths as a function of Lyapunov index has a distinct shape in the low density limit $\rho \to 0$ with a critical value ζ_{EL} of the Lyapunov index where the localization

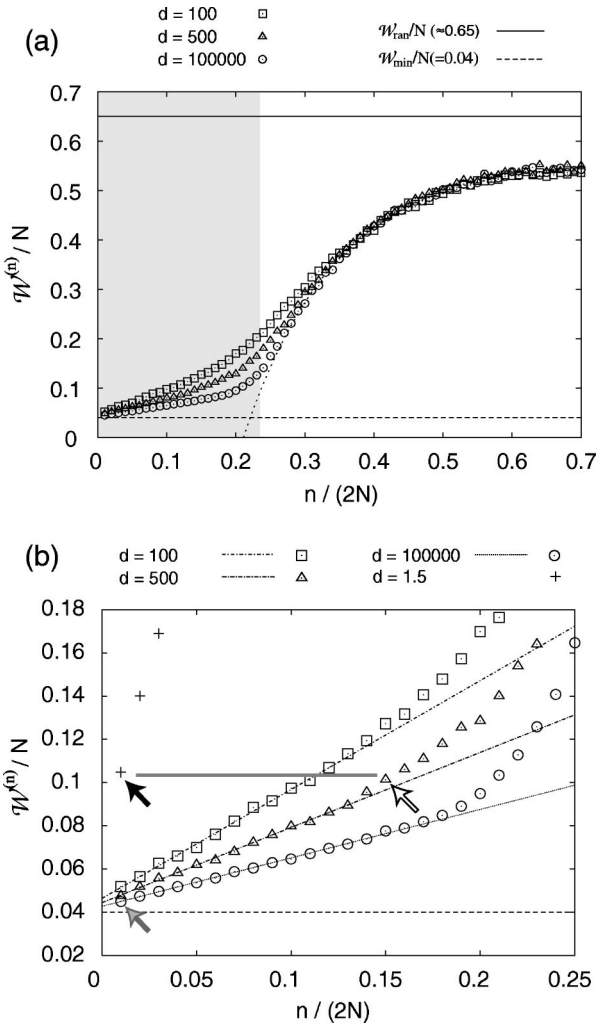

FIG. 7. Normalized localization widths $\mathcal{W}^{(n)}/N$ as functions of the normalized Lyapunov index $n/(2N)$ in the low density cases $d = 10^2$ (squares), $d = 5\times10^2$ (triangles), and $d = 10^5$ (circles). The localization widths $\mathcal{W}^{(n)} = \mathcal{W}_{ran}$ and $\mathcal{W}_{min}$ are indicated by the solid line and the dashed line, respectively. (a) Localization widths in the Lyapunov index region $n/(2N) \leqslant 0.7$. The data are fitted by an exponential function. The gray region is the region in which the localization widths show a linear dependence $[\mathcal{L}D]$ as a function of Lyapunov index in the low density limit. (b) Enlarged graphs including the linear dependence region of the localization widths. The data are fitted by linear functions. This figure also includes a part of the graph of the normalized localization widths for the case $d = 1.5$ (crosses), which has already been shown in Fig. 6. The localization widths indicated by the black arrow, the gray arrow, and the outline arrow correspond to localized behaviors of the Lyapunov vectors shown in Figs. 2(a), 2(b), and 8, respectively. The thick gray horizontal line to connect the localization widths indicated by the black arrow and the outline arrow in Fig. (b) is given to show that these values take almost the same value.

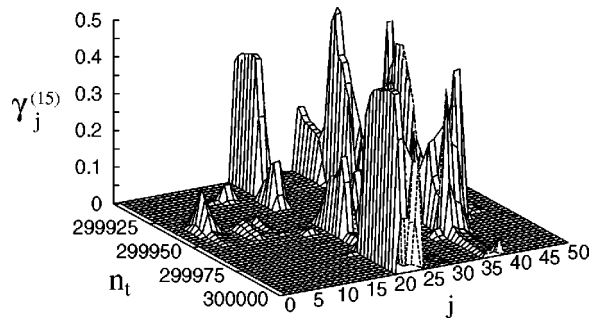

FIG. 8. Localized behaviors of the amplitudes $\gamma_j^{(15)}$ of the normalized Lyapunov vector components of each particle as a function of the collision number n_t and the particle index j for $d=5\times10^2$. The corresponding localization width is indicated by the outline arrow in Fig. 7(b).

width $\mathcal{W}^{(n)}$ shows a linear dependence $[\mathcal{L}D]$ in the Lyapunov index $n\leqslant\zeta_{EL}$ and shows an exponential dependence $[\mathcal{E}D]$ in the Lyapunov index $n>\zeta_{EL}$.

It is important to note that the exponential dependence $[\mathcal{E}D]$ and the linear dependence $[\mathcal{L}D]$ of the localization widths can also be distinguished by the shapes of the amplitudes $\gamma_j^{(n)}(t)$ of the normalized Lyapunov vector components of each particle. To discuss this point we note that Fig. 2(a) is the localized behavior of the Lyapunov vector corresponding to the Lyapunov width indicated by the black arrow in Figs. 6 and 7(b) and is in the region of exponential dependence $[\mathcal{E}D]$ of localization widths. This localization shows a long tail behavior. On the other hand, Fig. 2(b) is the Lyapunov localization corresponding to the localization width indicated by the gray arrow in Fig. 7(b) and is in the region of linear dependence $[\mathcal{L}D]$ of localization widths. This localization shows a sharp rectangular shape (with width 2). These observations lead to the conjecture that in the exponential dependence $[\mathcal{E}D]$ the amplitudes $\gamma_j^{(n)}(t)$ have a long tail, and in the linear dependence $[\mathcal{L}D]$ the amplitudes $\gamma_j^{(n)}(t)$ have a rather sharp rectangular shape. To make this point convincing, we compare the behaviors of the amplitudes $\gamma_j^{(n)}(t)$ corresponding to two localization widths, which take almost the same value of the localization widths but show different dependences $[\mathcal{L}D]$ and $[\mathcal{E}D]$ of the localization widths. For this purpose we choose the 15th localization width $\mathcal{W}^{(15)}$ for $d=5\times10^2$. This localization width, indicated by the outlined arrow in Fig. 2(b), is in the region of the linear dependence $[\mathcal{L}D]$ and takes almost the same value as the localization width $\mathcal{W}^{(1)}$ indicated by the black arrow in Figs. 6 and 7(b) in the case $d=1.5$, which is in the region of exponential dependence $[\mathcal{E}D]$ of the localization widths, and whose localized behavior is shown in Fig. 2(a). Figure 8 shows the localized behavior of the amplitudes $\gamma_j^{(15)}(t)$ as a function of the collision number n_t and the particle index j for $d=5\times10^2$. Here, the data in Fig. 8 are taken after every second collision. This figure shows that some peaks of the amplitudes $\gamma_j^{(n)}(t)$ have flat tops with a width 2 and distinct rectangular shapes, although its corresponding Lyapunov exponent, the 15th Lyapunov exponent, is far from the largest one and is less localized than in Fig. 2.

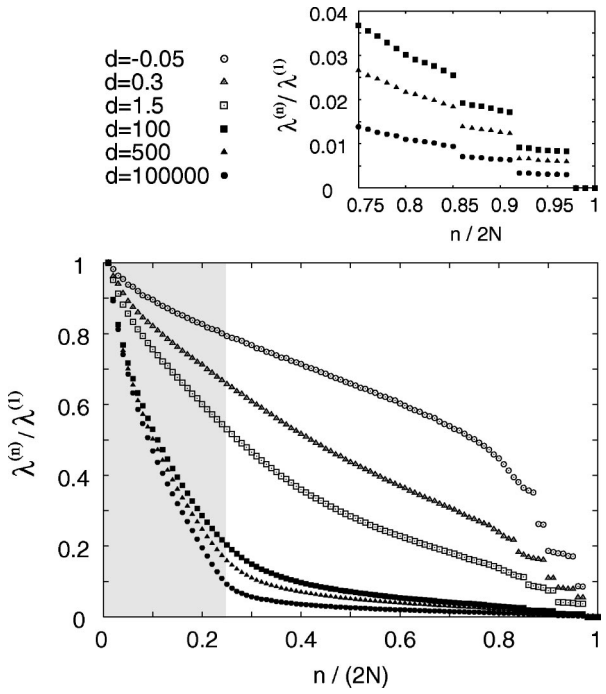

FIG. 9. Lyapunov spectra normalized by the largest Lyapunov exponents $\lambda^{(1)}$ as functions of the normalized Lyapunov index $n/(2N)$ for $d=-5\times10^{-2}$ (open circles), $d=0.3$ (open triangles), $d=1.5$ (open squares), $d=10^2$ (closed squares), $d=5\times10^2$ (closed triangles), and $d=10^5$ (closed circles). The gray region is the region in which the localization widths show a linear dependence $[\mathcal{L}D]$ as a function of the Lyapunov index at low densities. The small figure in the upper right side shows the enlarged graphs of the small positive region of the Lyapunov spectra for the low density cases of $d=10^2$, 5×10^2, and 10^5.

It should be noted that the linear dependence $[\mathcal{L}D]$ of the localization widths as a function of the Lyapunov index is not a property of the quasi-one-dimensional systems only. In Appendix B we consider the localization widths in a square system, and show that the linear dependence $[\mathcal{L}D]$ of the Lyapunov localization also appears in the square system.

IV. LYAPUNOV SPECTRA AND THE ANGLES AND AMPLITUDES OF LYAPUNOV VECTOR COMPONENTS

In this section, we consider how differences between the linear $[\mathcal{L}D]$ and exponential dependences $[\mathcal{E}D]$ of the localization widths affect other quantities, such as the Lyapunov spectrum, the angle between the spatial and momentum parts of the Lyapunov vectors, and the amplitudes of the x and y components of the spatial part and the momentum part of the Lyapunov vectors. We also investigate the effects of the stepwise structure of the Lyapunov spectra on these quantities.

A. Lyapunov spectra

Figure 9 shows the normalized Lyapunov spectra for the systems as functions of the normalized Lyapunov index for a range of values of d. Here the values of the largest Lyapunov exponents are given by $\lambda^{(1)}\approx4.79$ for $d=-5\times10^{-2}$, $\lambda^{(1)}$

≈ 1.64 for $d=0.3$, $\lambda^{(1)} \approx 0.769$ for $d=1.5$, $\lambda^{(1)} \approx 0.0579$ for $d=10^2$, $\lambda^{(1)} \approx 0.0161$ for $d=5\times 10^2$, and $\lambda^{(1)} \approx 0.000\,157$ for $d=10^5$. The negative branch of the Lyapunov spectra are omitted in this figure because of the conjugate property (12) of the Lyapunov exponents. The Lyapunov index dependences of the localization widths in these cases were shown in Figs. 6 and 7. It should be emphasized that in the low density cases, in which the linear dependence $[\mathcal{L}D]$ appears, we can recognize a sharp bend in the Lyapunov spectra around the normalized Lyapunov index $n=\zeta_{EL}$. Such a bending point corresponds to the point that distinguishes the dependences $[\mathcal{L}D]$ and $[\mathcal{E}D]$ of the localization widths in Fig. 7. (In this figure the region of the linear dependence $[\mathcal{L}D]$ of localization widths at low densities has a gray background.) It may be noted that such a bending of the Lyapunov spectrum has also been reported in a fully two-dimensional system [33] (also see the Lyapunov spectra for the Fermi-Pasta-Ulam models in Refs. [34,35]).

In Fig. 9 we can see some stepwise structures of the Lyapunov spectra, not only in the high density cases $d=-5\times 10^{-2}$, $d=0.3$ and 1.5, but also in the low density cases $d=10^2$, $d=5\times 10^2$ and $d=10^5$. (See the enlarged graphs in the upper right side of Fig. 9 for the stepwise structure of the Lyapunov spectra in these low density cases.) The steps of the Lyapunov spectra consist of two-point steps and four-point steps, which were considered in Ref. [25] in detail. Different from the high density cases, at low density the separations of the two-point steps and the four-point steps in the Lyapunov spectra are not so clear.

B. Angle between the spatial and the momentum parts of the Lyapunov vectors

As a second example to illustrate the effects of the two dependences $[\mathcal{L}D]$ and $[\mathcal{E}D]$ of localization widths, we consider the angle $\theta^{(n)}$ between the spatial part $\delta\mathbf{q}^{(n)}=(\delta\mathbf{q}_1^{(n)},\delta\mathbf{q}_2^{(n)},\ldots,\delta\mathbf{q}_N^{(n)})^T$ and the momentum part $\delta\mathbf{p}^{(n)}=(\delta\mathbf{p}_1^{(n)},\delta\mathbf{p}_2^{(n)},\ldots,\delta\mathbf{p}_N^{(n)})^T$ of the Lyapunov vector $\delta\mathbf{\Gamma}^{(n)}$ corresponding to the nth Lyapunov exponent $\lambda^{(n)}$, which is defined by

$$\theta^{(n)} \equiv \cos^{-1}\left(\frac{\delta\mathbf{q}^{(n)}\cdot\delta\mathbf{p}^{(n)}}{|\delta\mathbf{q}^{(n)}||\delta\mathbf{p}^{(n)}|} \right). \tag{15}$$

Noting the conjugate relations

$$\frac{\delta\mathbf{q}^{(4N-n+1)}\cdot\delta\mathbf{p}^{(4N-n+1)}}{|\delta\mathbf{q}^{(4N-n+1)}||\delta\mathbf{p}^{(4N-n+1)}|} = -\frac{\delta\mathbf{q}^{(n)}\cdot\delta\mathbf{p}^{(n)}}{|\delta\mathbf{q}^{(n)}||\delta\mathbf{p}^{(n)}|} \tag{16}$$

following from the conjugate property (11) of the Lyapunov vectors, the angle $\theta^{(n)}$ satisfies the condition

$$\theta^{(4N-n+1)} = \pi - \theta^{(n)}. \tag{17}$$

This angle has already been investigated in many-particle systems [7,25]. It should be noted that some analytical approaches give a formula to calculate Lyapunov exponents from the spatial part only (or the momentum part only) of the tangent vector [8,36,37], so it is important to investigate the relation between the spatial part and the momentum part of the Lyapunov vector.

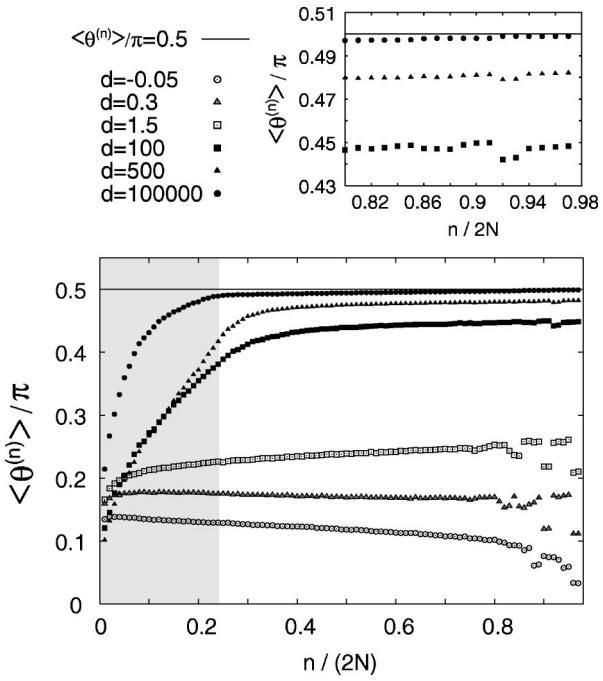

FIG. 10. The time average $\langle\theta^{(n)}\rangle/\pi$ of the angle divided by π for the spatial part $\delta\mathbf{q}^{(n)}$ and the momentum part $\delta\mathbf{p}^{(n)}$ of the Lyapunov vector corresponding to the nth Lyapunov exponent $\lambda^{(n)}$ as functions of the normalized Lyapunov index $n/(2N)$ for $d=-5\times 10^{-2}$ (open circles), $d=0.3$ (open triangles), $d=1.5$ (open squares), $d=10^2$ (closed squares), $d=5\times 10^2$ (closed triangles), and $d=10^5$ (closed circles). The gray region is the region in which the localization widths show a linear dependence $[\mathcal{L}D]$ as a function of the Lyapunov index in low density cases. The solid line corresponds to the value $\theta^{(n)}=\pi/2$ of the angle. The small figure in the upper right side shows the enlarged graphs for the low density cases $d=10^2$, 5×10^2, and 10^5 in the region of large Lyapunov indices.

In Fig. 10 we show the graphs of the time average $\langle\theta^{(n)}\rangle/\pi$ as a function of the normalized Lyapunov index $n/(2N)$ for a range of values of d. Here the time average of the angle $\theta^{(n)}$ is the arithmetic average of their values immediately after collision, for $1000N$ collisions. The plots of the time-averaged angles $\langle\theta^{(n)}\rangle$, $n=2N+1,2N+2,\ldots,4N$, corresponding to the negative branch of the Lyapunov exponents are omitted because of the conjugate property (17) of the angle $\theta^{(n)}$. It is noted that in our numerical calculations the amplitudes $|\delta\mathbf{p}^{(n)}|$, $n=2N-2$, $2N-1$, and $2N$ corresponding to zero-Lyapunov exponents are zero (or extremely small), so the angles $\theta^{(n)}$, $n=2N-2$, $2N-1$, and $2N$ cannot be defined. This is the reason why we do not plot these angles in Fig. 10 (see Sec. IV C about this point). This figure shows that in the low density cases, in which the linear dependence $[\mathcal{L}D]$ of the localization widths appears, the spectra of the averaged angle $\langle\theta^{(n)}\rangle$ bend around the value $n/(2N)=\zeta_{EL}/(2N)$ of the normalized Lyapunov index. (In Fig. 10 we showed a region of the linear dependence $[\mathcal{L}D]$ of the localization widths as a gray region.) In the region of

the linear dependence $[\mathcal{L}D]$ of the localization widths the time-averaged angles $\langle\theta^{(n)}\rangle$ increase monotonically as functions of Lyapunov indices n, while the time-averaged angles $\langle\theta^{(n)}\rangle$ corresponding to the exponential dependence $[\mathcal{E}D]$ of the localization widths are close to $\pi/2$, meaning that in this region the vector $\delta\mathbf{q}^{(n)}$ is almost orthogonal to the vector $\delta\mathbf{p}^{(n)}$ (see the case of $d=10^5$ in Fig. 10).

We can also see the effect of the stepwise structure of the Lyapunov spectra in the angle $\theta^{(n)}$. As shown in Fig. 10 the values of the time-averaged angles $\langle\theta^{(n)}\rangle$ corresponding to the two-point steps of the Lyapunov spectra in Fig. 9 are rather smaller than the values corresponding to their four-point steps, at all densities shown in Fig. 10 (see the upper right side of Fig. 10 for the low density cases). Therefore the Lyapunov index dependence of the time-averaged angles $\langle\theta^{(n)}\rangle$ can be used to distinguish the two-point step of the Lyapunov spectra from the other parts.

C. Amplitudes of the *x* and *y* components of the Lyapunov vectors

As shown in Sec. IV A, in low density cases the positive branch of Lyapunov spectra is separated into three parts: (i) A region in which the Lyapunov spectrum is a rapidly decreasing function of the Lyapunov index and corresponds to the linear dependence $[\mathcal{L}D]$ of the localization widths; (ii) a region in which the values of the Lyapunov exponents are very small compared to the largest Lyapunov exponent and correspond to the exponential dependence $[\mathcal{E}D]$ of the localization widths, and (iii) a region showing the stepwise structure of the Lyapunov spectra. The boundaries of regions (i) and (ii) of the Lyapunov spectra appear as a sharp bending of the Lyapunov spectra in the low density limit. To understand this characteristic of the Lyapunov spectra we note that a positive Lyapunov exponent is connected to a decorrelation rate in chaotic dynamics, and a larger positive Lyapunov exponent means that a trajectory diverges more rapidly on the energy surface in ergodic systems and loses correlation with its initial value more quickly. This is partly supported by the fact that the Kolmogorov-Sinai entropy, which is equal to the sum of all the positive Lyapunov exponents (Pesin's identity) in closed systems, is connected to the inverse relaxation time in ergodic systems [1]. A relation between a Lyapunov exponent and a decay rate of time correlation is also discussed in Refs. [38,39]. Another example of a relation between a time scale of the dynamics and a positive Lyapunov exponent is the tracer particle effect in Lyapunov spectra [40]. On this subject, a many-particle system consisting of a small light particle, called the tracer particle, moving at high speed (the short time scale) and many big heavy particles moving at low speeds (the long time scale) is considered. It is shown that the existence of the tracer particle leads to relatively large Lyapunov exponents compared with the Lyapunov exponents corresponding to the other heavy particles. At low density the quasi-one-dimensional systems exhibit a bending of the Lyapunov spectra, which separates the set of positive Lyapunov exponents into two groups (i) and (ii) of relatively different values, and this suggests the existence of a time-scale separation in the dynamics of these systems.

One might think that in the quasi-one-dimensional systems such a time-scale separation may come from the very narrow rectangular shape of the system. In the quasi-one-dimensional system, especially in the large d case with a low density, the time-scale of oscillation of each particle in the x direction is much larger than the time scale of that in the y direction, and it may be one possibility leading to the time-scale separation mentioned above. (However this possibility may be rather unlikely, because as shown in Appendix the bending point of the Lyapunov spectra does not change significantly on changing the system from quasi-one-dimensional to square with the same area L_xL_y and the same number of particles N.) Another possibility to explain this bending of the Lyapunov spectrum may be from the different roles of the spatial and momentum parts of the Lyapunov vectors at low density. The result in Sec. IV B supports this point, showing that the spatial and momentum parts of the Lyapunov vectors are not in the same direction at low density.

Motivated by the above considerations, in this section we consider the amplitudes of the four parts of the Lyapunov vectors: the x and y components in the spatial part and the momentum part of the Lyapunov vectors, namely, the four kinds of quantities defined by

$$\eta_{qj}^{(n)}(t)\equiv\frac{\sum_{k=1}^{N}|\delta q_{jk}^{(n)}(t)|^2}{\sum_{k=1}^{N}|\delta\mathbf{\Gamma}_k^{(n)}(t)|^2}, \tag{18}$$

$$\eta_{pj}^{(n)}(t)\equiv\frac{\sum_{k=1}^{N}|\delta p_{jk}^{(n)}(t)|^2}{\sum_{k=1}^{N}|\delta\mathbf{\Gamma}_k^{(n)}(t)|^2}, \tag{19}$$

$j=x$ and y, in each Lyapunov index n. Here $\delta q_{jk}^{(n)}(t)$ and $\delta p_{jk}^{(n)}(t)$ are the j components of the spatial coordinate part $\delta\mathbf{q}_k^{(n)}=(\delta q_{xk}^{(n)}(t),\delta q_{yk}^{(n)}(t))$ and the momentum part $\delta\mathbf{p}_k^{(n)}=(\delta p_{xk}^{(n)}(t),\delta p_{yk}^{(n)}(t))$ of the Lyapunov vector $\delta\mathbf{\Gamma}_k^{(n)}=(\delta\mathbf{q}_k^{(n)},\delta\mathbf{p}_k^{(n)})$ corresponding to the kth particle and the nth Lyapunov exponent at time t, respectively. These four quantities are normalized as

$$\eta_{px}^{(n)}(t)+\eta_{py}^{(n)}(t)+\eta_{qx}^{(n)}(t)+\eta_{qy}^{(n)}(t)=1 \tag{20}$$

by their definitions. Using the conjugate property (11) of the Lyapunov vector we obtain

$$\eta_{pj}^{(4N-n+1)}(t)=\eta_{qj}^{(n)}(t), \tag{21}$$

$$\eta_{qj}^{(4N-n+1)}(t)=\eta_{pj}^{(n)}(t). \tag{22}$$

Therefore we can omit the quantities $\eta_{pj}^{(4N-n+1)}(t)$ and $\eta_{qj}^{(4N-n+1)}(t)$, for $n=1,2,\ldots,2N$ corresponding to the negative branch of the Lyapunov spectra.

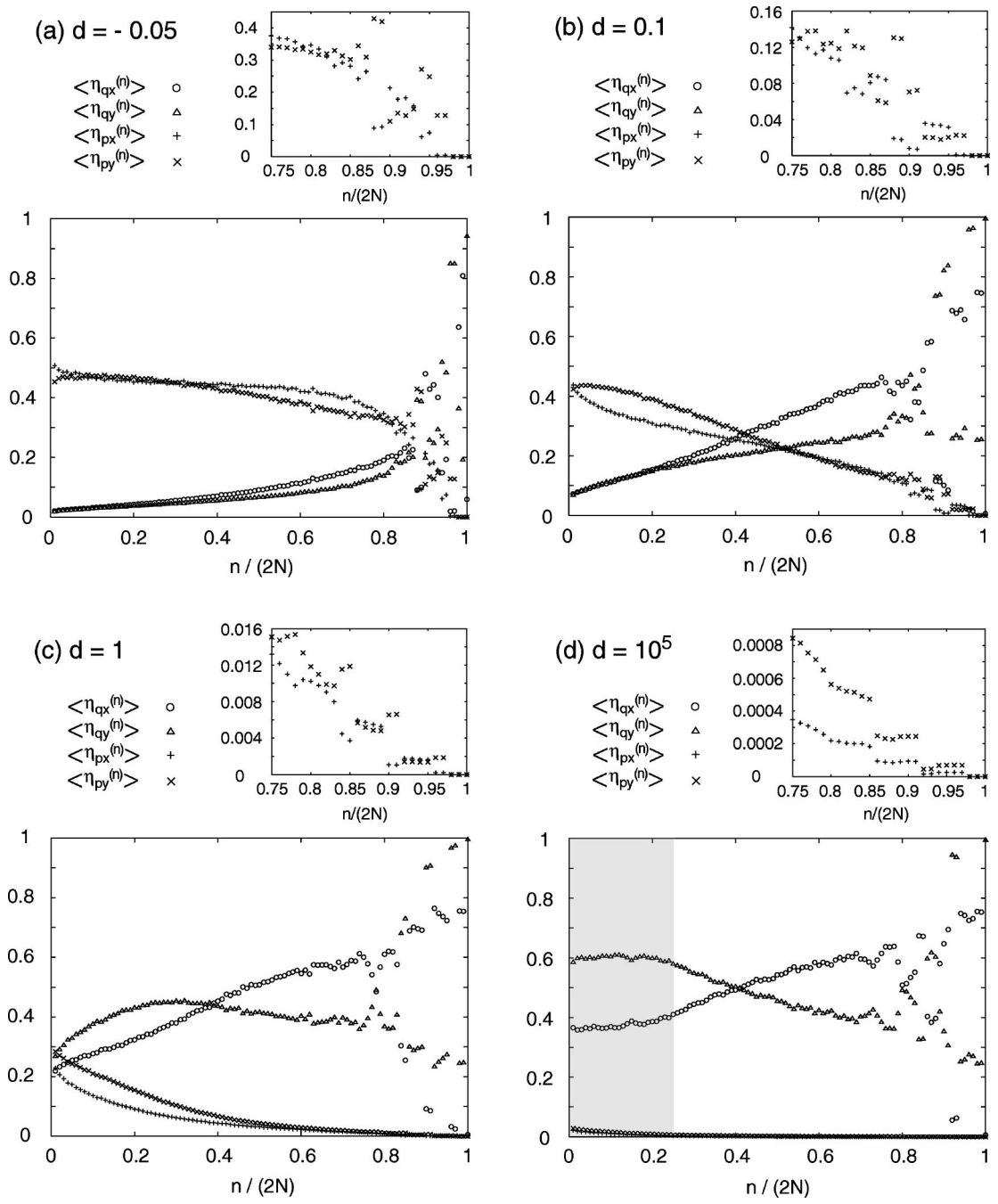

FIG. 11. The time averages of the normalized amplitudes of the x component of the spatial part $[\langle \eta_{qx}^{(n)}(t)\rangle$, circles], the y component of the spatial coordinate part $[\langle \eta_{qy}^{(n)}(t)\rangle$, triangles], the x component of the momentum part $[\langle \eta_{px}^{(n)}(t)\rangle$, pulses], and its y component of the momentum part $[\langle \eta_{py}^{(n)}(t)\rangle$, crosses] of the Lyapunov vectors as functions of the normalized Lyapunov index $n/(2N)$ for $d=-5\times10^{-2}$ [graph (a)], $d=0.1$ [graph (b)], $d=1$ [graph (c)], and $d=10^5$ [graph (d)]. The small panels in the top right of (a), (b), (c). and (d) are enlarged graphs of $\langle \eta_{px}^{(n)}(t)\rangle$ and $\langle \eta_{py}^{(n)}(t)\rangle$ in the small positive Lyapunov exponent regions. The gray region in graph (d) is the region in which the localization widths show a linear dependence $[\mathcal{L}D]$ as a function of the Lyapunov index.

Figure 11 contains the graphs of the time-averaged quantities defined by Eqs. (18) and (19) as functions of the normalized Lyapunov index $n/(2N)$ for a range of values of d. Here the time average $\langle \mathcal{X}\rangle$ of the quantities $\mathcal{X}=\eta_{qx}^{(n)}(t)$, $\eta_{qy}^{(n)}(t)$ $\eta_{px}^{(n)}(t)$ and $\eta_{py}^{(n)}(t)$ are taken as the arithmetic average of the quantity $\mathcal{X}$ immediately after collisions, for $1000N$ collisions. The cases of $d=-5\times10^{-2}$ and $d=10^5$ shown in Figs. 11(a) and 11(d) are the cases of the highest density and the lowest density, respectively, considered in Secs. III, IV A, and IV B, and the other two cases are given to show intermediate situations between the two cases of Figs. 11(a) and 11(d). It is noted that Figs. 11(a)–11(c) are for the case of a particle density in which the linear dependences $[\mathcal{L}D]$ of localization widths do not appear yet, and only in the gray region of Figs. 11(d) does the linear dependence $[\mathcal{L}D]$ appear. From this figure it is clear that there is a strong asym-

metry between the spatial and momentum parts of the Lyapunov vectors in any density region, as well as an asymmetry between the x and y components of the Lyapunov vectors especially at low density.

The behavior of the graphs in Fig. 11 are different in the region where the Lyapunov spectra change smoothly and in the stepwise region of the Lyapunov spectra. First we discuss the region where the Lyapunov spectra change smoothly, which is the region of the Lyapunov indexes $n/(2N)<0.8$ approximately in Fig. 11. In the high density case shown in Fig. 11(a) the momentum parts ($\langle \eta_{px}^{(n)}(t)\rangle$ and $\langle \eta_{py}^{(n)}(t)\rangle$) of the Lyapunov vectors are larger than the corresponding spatial parts ($\langle \eta_{qx}^{(n)}(t)\rangle$ and $\langle \eta_{qy}^{(n)}(t)\rangle$). As the density decreases, the spatial parts of the Lyapunov vectors increase (and momentum parts decrease), first in the *small* positive Lyapunov exponent region [see changes from Fig. 11(a) to Fig. 11(b)], and then in the *large* Lyapunov exponent region [see changes from Fig. 11(b) to Fig. 11(d) via Fig. 11(c)]. At very low density, as shown in Fig. 11(d), the spatial parts of the Lyapunov vectors are much larger than the corresponding momentum parts for Lyapunov vectors of any index, and a linear dependence [$\mathcal{L}D$] of the localization widths appears. In this density region a significant gap in the x and y components of the spatial part of the Lyapunov vectors appears, and the transverse part [$\langle \eta_{qy}^{(n)}(t)\rangle$] is larger than the longitudinal part $\langle \eta_{qx}^{(n)}(t)\rangle$ in the large positive Lyapunov exponent region while the reverse is true in the small positive Lyapunov exponent region. In the low density limit the momentum parts $\langle \eta_{px}^{(n)}(t)\rangle$ and $\langle \eta_{py}^{(n)}(t)\rangle$ are extremely small so the spatial parts $\langle \eta_{qx}^{(n)}(t)\rangle$ and $\langle \eta_{qy}^{(n)}(t)\rangle$ are almost symmetric in the line $y=0.5$ as required by the normalization condition (20). It should be emphasized that in the Lyapunov index of the linear dependence [$\mathcal{L}D$] of the localization widths the quantities $\langle \eta_{qy}^{(n)}(t)\rangle$ and $\langle \eta_{qx}^{(n)}(t)\rangle$ are rather flat, shown in the gray region in Fig. 11(d). We can show that these asymmetries between the x and y components of the Lyapunov vectors actually come from its narrow rectangular shape, because as shown in Appendix B such asymmetries do not appear in the square system, although the asymmetries between the spatial and momentum parts of the Lyapunov vectors still exist there.

As a second point, Fig. 11 also shows some characteristics of the time-averaged amplitudes of the Lyapunov vector components corresponding to the stepwise region of the Lyapunov spectra. In Fig. 11 we can see flat parts consisting of two-points (four-points) for the time-averaged normalized amplitudes $\langle \eta_{qx}^{(n)}(t)\rangle$, $\langle \eta_{qy}^{(n)}(t)\rangle$, $\langle \eta_{px}^{(n)}(t)\rangle$ and $\langle \eta_{py}^{(n)}(t)\rangle$ of the Lyapunov vectors, which correspond to the two-point steps (the four-point steps) of the Lyapunov spectra (see Figs. 11(a)–11(d) in the region of the Lyapunov index around $n/(2N)>0.9$, as well as the small panels in the top right of these figures for enlarged momentum parts $\langle \eta_{px}^{(n)}(t)\rangle$ and $\langle \eta_{py}^{(n)}(t)\rangle$ in the small positive Lyapunov exponent regions). Values of the two-point steps of the transverse part $\langle \eta_{qy}^{(n)}(t)\rangle$ and $\langle \eta_{py}^{(n)}(t)\rangle$ of the Lyapunov vectors corresponding to the two-point steps of the Lyapunov spectra are larger than their longitudinal parts $\langle \eta_{qx}^{(n)}(t)\rangle$ and $\langle \eta_{px}^{(n)}(t)\rangle$ in Figs. 11(a)–11(d). On the other hand, values of the four-point steps of the longitudinal part $\langle \eta_{qx}^{(n)}(t)\rangle$ and $\langle \eta_{px}^{(n)}(t)\rangle$ of the Lyapunov vectors corresponding to the four-point steps of the Lyapunov spectra are larger than their transverse parts $\langle \eta_{qy}^{(n)}(t)\rangle$ and $\langle \eta_{py}^{(n)}(t)\rangle$ in Figs. 11(a)–11(c), and the spatial parts of the Lyapunov vectors in Figs. 11(d). At any density the spatial parts $\langle \eta_{qx}^{(n)}(t)\rangle$ and $\langle \eta_{qy}^{(n)}(t)\rangle$ are usually larger than the momentum parts $\langle \eta_{px}^{(n)}(t)\rangle$ and $\langle \eta_{py}^{(n)}(t)\rangle$, respectively, in the region of Lyapunov indices indicating the stepwise structure of the Lyapunov spectra. It should be emphasized that wavelike structure (the transverse Lyapunov modes) in the y components of the spatial part and the momentum part of the Lyapunov vectors appears in the two-point steps of the Lyapunov spectra reported by Refs. [5,25], and Fig. 11 suggests that we may get a rather clearer wavelike structure in the spatial part of the Lyapunov vectors than in its momentum part. We can conclude a similar result for the four-point steps of the Lyapunov spectra in which time-dependent wavelike structure in the y components of the spatial part of the Lyapunov vectors and in x components of the spatial part of the Lyapunov vectors [16,25] is observed. It may be noted that the time-averaged amplitudes $\langle \eta_{px}^{(n)}(t)\rangle$ and $\langle \eta_{py}^{(n)}(t)\rangle$, $n=2N-2$, $2N-1$, and $2N$ corresponding to zero Lyapunov exponents are almost zero at any density (see the small panels in the top right of Figs. 11(a)–11(d)).

V. DENSITY DEPENDENCE OF THE LARGEST LYAPUNOV EXPONENT AND RELATED QUANTITIES

As we have already shown in Sec. III, the linear dependence [$\mathcal{L}D$] of localization widths as a function of the Lyapunov index appears at low density, but it was not clear at what density the linear dependence [$\mathcal{L}D$] of the Lyapunov localization first appears as the particle density ρ deceases from 1. In this section we discuss this problem by calculating the density dependences of the largest Lyapunov exponent, the angle and amplitudes of Lyapunov vector components, and the localization width, which correspond to the largest Lyapunov exponent. Especially, we show that the particle density region in which the linear dependence [$\mathcal{L}D$] appears is almost the same as the density region in which the largest Lyapunov exponent begins to satisfy the Krylov relation.

A. Largest Lyapunov exponent

Figure 12 shows the largest Lyapunov exponent $\lambda^{(1)}$ as a function of the density ρ in the quasi-one-dimensional system. In this figure we show the numerical error at each data point as an error bar. Clearly the value of the largest Lyapunov exponent at very low densities is less accurate than that at higher densities. The gray region in this figure is the density region in which the linear dependence [$\mathcal{L}D$] of the localization widths appears.

It is known that in the low density limit the largest Lyapunov exponent $\lambda^{(1)}$ should have the form

$$\lambda^{(1)} \sim \alpha\rho \ln(\beta\rho) \tag{23}$$

with parameters α and β. Equation (23) is called the Krylov relation [41] and has already been demonstrated numerically in a fully two-dimensional (three-dimensional) system con-

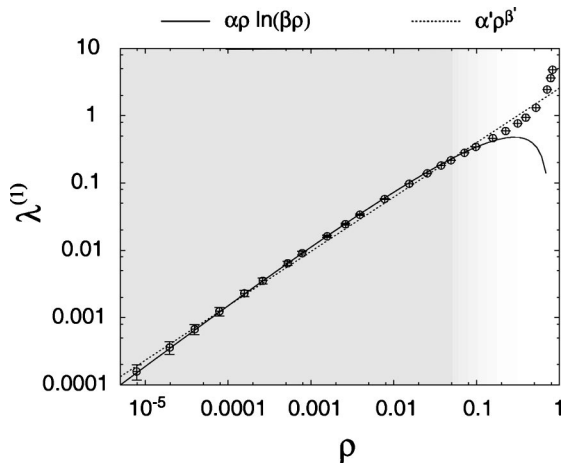

FIG. 12. Largest Lyapunov exponent $\lambda^{(1)}$ as a function of particle density ρ. The gray region is the density region in which the linear dependence $[\mathcal{L}D]$ of the localization widths as a function of the Lyapunov index appears. Numerical data are fitted by the Krylov relation $\lambda^{(1)} \sim \alpha\rho\ln(\beta\rho)$ (solid line) and the power function $y = \alpha' \rho^{\beta'}$ (dashed line) with fitting parameters α, β, α', and β'. The error bar in each data point is given by the absolute value $2|\lambda^{(1)} + \lambda^{(4N)}|$ or twice of the sum of the largest and the smallest Lyapunov exponent.

sisting of many-hard-disks (many-hard-spheres) [31,42], apart from a factor. In Fig. 12 we fitted the numerical data to the Krylov relation (23) with parameter values $\alpha = -1.668\,75$ and $\beta = 1.282\,52$ (the solid line), which gives a good fit for the density dependence of the largest Lyapunov exponent. It is important to note that the density region where the largest Lyapunov exponent satisfies the Krylov relation almost exactly coincides with the density region in which the linear dependence $[\mathcal{L}D]$ of the localization widths appears. To test the Krylov relation (23), we also tried to fit the numerical data by a power law $y = \alpha' \rho^{\beta'}$ (dashed line) with fitting parameters α' and β' in Fig. 12. We used the parameter values $\alpha' = 2.551\,26$ and $\beta' = 0.808\,158$, and it is shown in Fig. 12 that the Krylov relation (23) gives a better fit than this power law in the gray region.

Now we check the values of the fitting parameters α and β used to fit the graph of Fig. 12 by following the rough derivation of the Krylov relation in Ref. [1]. (Note that more exact derivations are known for some specific systems, such as the Lorentz gas, etc. See, for example, Refs. [43,44].) First we note that after n_t particle collisions the amplitude of a Lyapunov vector is stretched by a factor $(l_f/R)^{n_t}$ approximately with l_f the mean free path. Introducing the collision rate $\nu \equiv n_t/t$ to connect the mean free path l_f with the time t we estimate the largest Lyapunov exponent as

$$\lambda^{(1)} \sim \lim_{t \to +\infty} \frac{1}{t} \ln \left(\frac{l_f}{R} \right)^{n_t} = \nu \ln \frac{l_f}{R}. \tag{24}$$

We approximate the collision rate ν by a thermal velocity $u_{th} \equiv \sqrt{(2/M)(K/N)}$ as $\nu \sim u_{th}/l_f$ because of $u_{th} t \sim n_t l_f$, and assume that the mean free path l_f is inversely proportional to the density ρ, so we obtain

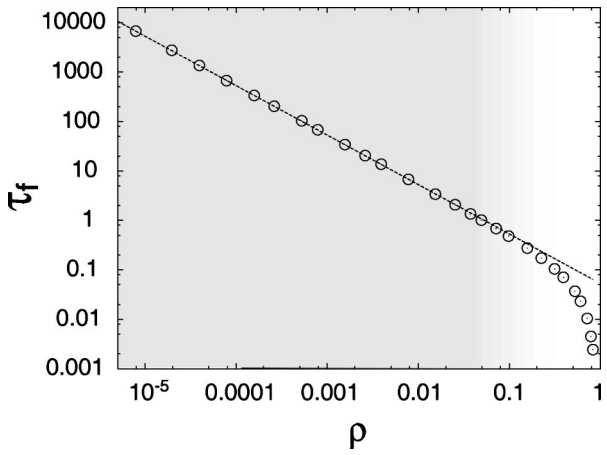

FIG. 13. Mean free time τ_f as a function of density ρ. The dotted line is a plot of the fitting function $y = 1/(u_{th}\gamma x)$ with the thermal velocity u_{th} and the fitting parameter γ. The gray region is the density region in which the linear dependence $[\mathcal{L}D]$ of the localization widths as a function of the Lyapunov index appears.

$$\lambda^{(1)} \sim -u_{th}\gamma\rho \ln(R\gamma\rho), \tag{25}$$

using a constant γ of $l_f \sim (\gamma\rho)^{-1}$. Comparing Eq. (25) with Eq. (23) we obtain the relation

$$\frac{\alpha}{\beta} \sim -\frac{u_{th}}{R}, \tag{26}$$

which is independent of the value of the constant γ. Using the parameter values $u_{th} = \sqrt{2}$ and $R = 1$ in our numerical calculations, we obtain $\alpha/\beta \sim -\sqrt{2} = -1.4142\ldots$, which is consistent with the values of the fitting parameters α and β in Fig. 12: $\alpha/\beta = -1.3011\ldots$.

Next we proceed to estimate the factor $\gamma = (l_f\rho)^{-1}$ from Fig. 13, the graph of the mean free time as a function of the density. Noting the relation $l_f \sim u_{th}\tau_{th}$, in this figure we fitted the numerical data by the function $y = 1/(u_{th}\gamma x)$ obtaining the value $\gamma = 13.341$ for the fitting parameter γ. (We emphasized that this function gives a nice fit in the density region in which the linear dependence $[\mathcal{L}D]$ of the Lyapunov localization appears.) However this value $\gamma = 13.341$, which is β in Eq. (23) in the case of $R = 1$, is about ten times as large as the fitting value of β used to fit the graph of Fig. 12. It may be noted that in order to derive expression (25) for the largest Lyapunov exponent we neglected some characteristics of the quasi-one-dimensional systems, such as the fact that in the quasi-one-dimensional system with a large value of the parameter d particles collide mainly head on and it is rather rare for particles to have grazing collisions with other particles. We should take these points into account to get a more precise expressions for the parameters α and β in Eq. (23) than in Eq. (25).

B. Angle and amplitudes of Lyapunov vector components

As the next example we consider the angle $\theta^{(1)}$ defined by Eq. (15) between the spatial and momentum parts of the Lyapunov vector corresponding to the largest Lyapunov ex-

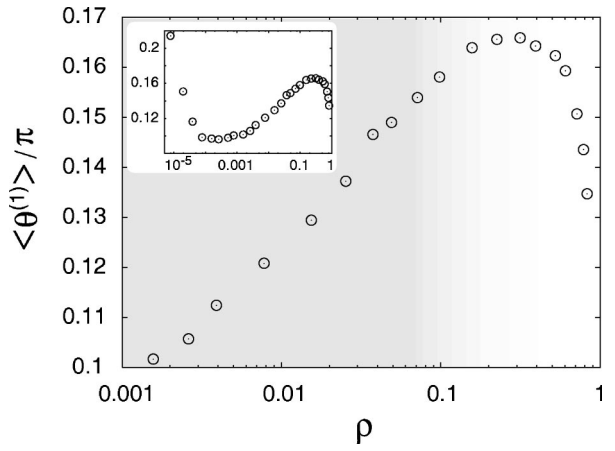

FIG. 14. The density dependence of the time-average $\langle \theta^{(1)} \rangle / \pi$, the angle between the spatial and momentum part of the Lyapunov vector of the largest Lyapunov exponent as a function of the particle density ρ. The gray region is the density region in which the linear dependence $[\mathcal{L}D]$ of the localization widths as a function of the Lyapunov index appears. The inset: The same graph but including the angle $\theta^{(1)}$ at lower density.

ponent. Figure 14 is the graph of the time average of the angle $\theta^{(1)}/\pi$ as a function of particle density ρ. The graph has a local maximum point at about $\rho \approx 0.2$, which is close to the value of particle density in which the linear dependence $[\mathcal{L}D]$ of the localization widths starts to appear as the density decreases from 1. As we have already discussed in Secs. II and III, the existence of the linear dependence $[\mathcal{L}D]$ of the localization widths can be checked by the linear dependence of the localization widths on the Lyapunov index and the rectangular shape of the amplitude of the Lyapunov vector, but it is rather hard to use this criterion to distinguish the density region of the linear dependence $[\mathcal{L}D]$, because it is not easy to recognize these behaviors in an intermediate region between the density region of the exponential dependence $[\mathcal{E}D]$ only and the density region of both the dependences $[\mathcal{E}D]$ and $[\mathcal{L}D]$. In this sense the graph of the angle $\theta^{(1)}$ as a function of particle density ρ may give a more distinct criterion to distinguish the density region in which the linear dependence $[\mathcal{L}D]$ appears. It is noted that the angle $\theta^{(1)}$ does not seem to go to zero in the low density limit as shown in the inset to Fig. 14.

Next in Fig. 15, we consider the density dependence of the time average of normalized amplitude of the x component and the y component of the spatial part and the momentum part of the Lyapunov vector corresponding to the largest Lyapunov exponent, which are defined by Eqs. (18) and (19) in $n=1$. This may not be a good criterion to distinguish the density region of the linear dependence $[\mathcal{L}D]$, but it is clear that in the density region of the linear dependence $[\mathcal{L}D]$ the spatial parts of the Lyapunov vector are dominant and a gap appears between its x component $\langle \eta_{qx}^{(1)}(t) \rangle$ and the y component $\langle \eta_{qy}^{(1)}(t) \rangle$. On the other hand, in the high density region in which the linear dependence $[\mathcal{L}D]$ does not appear, the momentum parts $\langle \eta_{px}^{(1)}(t) \rangle$ and $\langle \eta_{py}^{(1)}(t) \rangle$ of the Lyapunov vector are dominant. It should be noted that at the low density in which the linear dependence $[\mathcal{L}D]$ appears, the transverse components $\langle \eta_{qy}^{(1)}(t) \rangle$ and $\langle \eta_{py}^{(1)}(t) \rangle$ are always larger than the longitudinal components $\langle \eta_{qx}^{(1)}(t) \rangle$ and $\langle \eta_{px}^{(1)}(t) \rangle$, respectively.

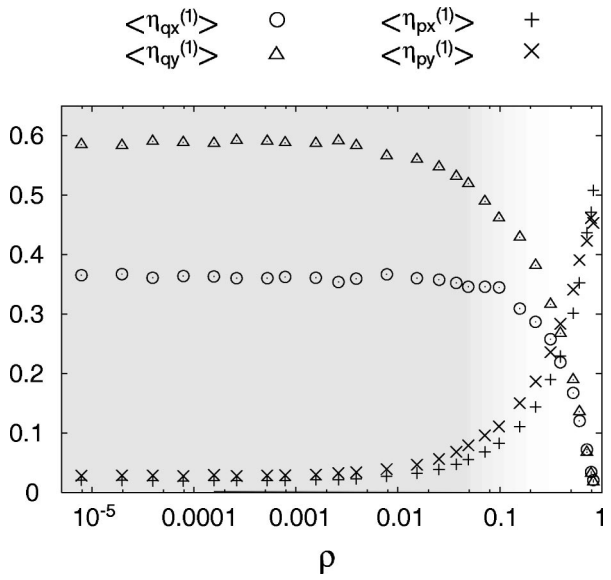

FIG. 15. The time averages of the normalized amplitudes of the x component of the spatial part $[\langle \eta_{qx}^{(1)}(t) \rangle$, circles], the y component of the spatial part $[\langle \eta_{qy}^{(1)}(t) \rangle$, triangles], the x component of the momentum part $[\langle \eta_{px}^{(1)}(t) \rangle$, pluses), and the y component of the momentum part $[\langle \eta_{py}^{(1)}(t) \rangle$, crosses] of the Lyapunov vector of the largest Lyapunov exponent as functions of the particle density ρ. The gray region is the density region in which the linear dependence $[\mathcal{L}D]$ of the localization widths as a function of the Lyapunov index appears.

C. Localization width

As the last quantity in this section, we consider the density dependence of the Lyapunov localization width corresponding to the largest Lyapunov exponent. Figure 16 is the graph of the Lyapunov localization width $\mathcal{W}^{(1)}/N$ normalized by the particle number N as a function of density ρ. This figure shows that in the low density limit the normalized localization width $\mathcal{W}^{(1)}/N$ goes to the value $2/N$ $(=0.04)$ (solid line in Fig. 16), which is discussed as the minimum localization width $\mathcal{W}_{min}/N$ in Sec. II. But it is not so clear from this figure how to distinguish the density region in which the linear dependence $[\mathcal{L}D]$ of the localization widths appears.

VI. CONCLUSION AND REMARKS

In this paper we have discussed localized behaviors of Lyapunov vectors (the Lyapunov localization) for quasi-one-dimensional systems consisting of many hard disks (with periodic boundary conditions except in Appendix B 5). The quasi-one-dimensional system was introduced as a particle system whose shape is a very narrow rectangle that does not allow the interchange of particle positions. We compared some methods to characterize the localized behavior of the Lyapunov vectors, and one such method used in this paper defines a quantity called the localization width, whose loga-

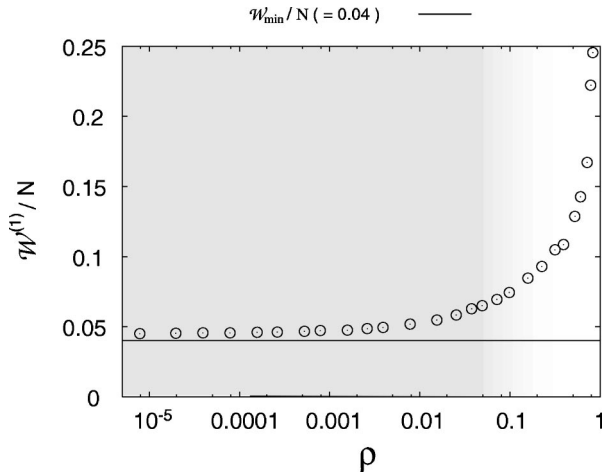

FIG. 16. The normalized localization width $\mathcal{W}^{(1)}/N$ for the largest Lyapunov exponent as a function of density ρ. The solid line is the minimum value of the normalized localization width: $\mathcal{W}_{min}/N = 0.04$. The gray region is the density region in which the linear dependence $[\mathcal{LD}]$ of the localization widths as a function of the Lyapunov index appears.

rithm is given by an entropy for the amplitude distribution of the Lyapunov vector components of each particle. The localization width indicates the number of particles contributing to the localized part of the Lyapunov vector. It could not only be used as an indicator to measure the magnitude of the localized behavior of the Lyapunov vectors, but also it can be used to distinguish different delocalized properties of the Lyapunov vectors such as the delocalization associated with a random distribution of particle component amplitudes, a delocalization associated with a uniform distribution, and a delocalization associated with a wavelike structure (corresponding to stepwise structure of the Lyapunov spectra) (Figs. 3 and 4). The localized region of the Lyapunov vectors is related to the positions of colliding particles (Fig. 5), and this leads to the lower bound 2 for the localization width (Figs. 7 and 16). Using the localization width we showed that there are two kinds of the Lyapunov localizations in many-hard-disk systems. The first type of the Lyapunov localization is that characterized by an exponential dependence $[\mathcal{ED}]$ of the localization width as a function of the Lyapunov index (Fig. 6), and by its long tail of localized Lyapunov vectors [Fig. 2(a)]. This type of the Lyapunov localization is observed at any particle density. The second type of the Lyapunov localization is characterized by the linear dependence $[\mathcal{LD}]$ of the localization widths as a function of the Lyapunov index (Fig. 7), and by the sharp rectangular shape of the localized Lyapunov vectors [Figs. 2(b) and 8]. This type of Lyapunov localization appears only in low density cases and in Lyapunov indices corresponding to the larger Lyapunov exponents (in absolute value). We showed that in the density region of the linear dependence $[\mathcal{LD}]$ of the localization widths the Lyapunov spectra are bent and separated into two parts (except for the stepwise region of the Lyapunov spectra): one corresponding to the exponential dependence $[\mathcal{ED}]$ and taking very small values corresponding to the largest Lyapunov exponent, and the other corresponding to the linear dependence $[\mathcal{LD}]$ and showing a rapid decreasing dependence of the Lyapunov index (Fig. 9). It was also shown that differences between the exponential dependence $[\mathcal{ED}]$ and the linear dependence $[\mathcal{LD}]$ appear in the angle $\theta^{(n)}$ between the spatial and momentum parts of the Lyapunov vectors (Fig. 10) and in the amplitudes of the x and y components of the spatial part [Fig. 11(d)]. (Here we took the y direction as the narrow direction of the rectangle and the x-direction as the longer orthogonal direction.) The density region, in which the linear dependence $[\mathcal{LD}]$ of localization widths appear, almost exactly coincides with the region in which the density dependence of the largest Lyapunov exponent $\lambda^{(1)}$ satisfies the Krylov relation (Fig. 12). We also indicated that at the boundary of the density region of the exponential dependence $[\mathcal{ED}]$ only and the density region of both the linear dependence $[\mathcal{LD}]$ and the exponential dependence $[\mathcal{ED}]$, the angle $\theta^{(1)}$ corresponding to the largest Lyapunov exponent shows a local maximum as a function of particle density (Fig. 14).

In this paper we observed differences in the amplitudes of the x and y components of the Lyapunov vectors (Figs. 11 and 15). These differences come from the difference in the roles of the directions in the quasi-one-dimensional systems. We also observed differences in the amplitudes of the spatial and momentum parts of the Lyapunov vectors. In the region where the Lyapunov spectra are changing smoothly the amplitude of the spatial part of the Lyapunov vectors is larger (smaller) than that of the momentum part in low (high) density cases (Figs. 11, 15, and 20). The spatial and momentum parts of the Lyapunov vectors are in almost the same direction at high density, whereas they are rather close to orthogonal in the low density case, especially in the region of the exponential dependence $[\mathcal{ED}]$ of the localization widths as a function of Lyapunov index (Figs. 10 and 19). These behaviors are found not only in the quasi-one-dimensional systems but also in the square system (Fig. 20). Concerning the stepwise region of the Lyapunov spectra, as shown in Fig. 11, the amplitudes of the y component (transverse component) of the spatial and momentum parts of the Lyapunov vectors are larger than the corresponding x components (their longitudinal components) in the two-point steps of the Lyapunov spectra, whereas they are opposite in four-point steps of the Lyapunov spectra [except in very low density cases as in Fig. 11(d)].

Microscopic chaos plays an essential role in the statistical treatments of deterministic dynamical systems, but it has also been noted that chaos is not a necessary condition for some particular statistical behaviors [45,46]. For instance, ergodicity does not require the system to be chaotic, and numerical work suggests that even some nonchaotic systems may exhibit the mixing property and thus guarantee the decay of correlations [47]. It has also been observed that nonchaotic systems can show diffusive behavior [48–52], Fourier's law of heat conduction [52], and satisfy the fluctuation theorem [53], which have all been regarded as important statistical properties of dynamical systems. As another example, many-particle effects are still of special interest in the statistical properties of dynamical systems, where it is observed that many particles are not necessary for systems to be chaotic

and even one-particle systems such as the Lorentz gas model and the billiard model [1,54] can show a positive Lyapunov exponent. The Lyapunov localization can be regarded as one of the many-particle effects.

The particle number dependence of the Lyapunov localization width normalized by the particle number N was investigated a little in this paper. Figure 3 suggests that the Lyapunov localization width normalized by the particle number decreases as a function of the particle number itself, but we need further calculations to show the existence of a thermodynamical limit ($N\rightarrow+\infty$), as well as its low density limit ($\rho\rightarrow 0$).

We suggested that the bending of the Lyapunov spectra in the low density cases accompanying the linear dependence [$\mathcal{L}D$] of the localization widths may come from a time-scale separation in the dynamics. As one of the possible explanations of this point we demonstrate a strong asymmetry of the amplitudes of the spatial and momentum parts of the Lyapunov vectors at low density. However this may not give a sufficient explanation as to where the bending point of the Lyapunov spectra is, and one may also indicate that the Lyapunov spectrum is related to growing (or reducing) speeds of the amplitudes of the Lyapunov vectors, not the amplitudes of the Lyapunov vectors themselves. This remains an open question.

In the Introduction we have noted the work on coupled map lattices Refs. [19–21], where a connection with the Kardar-Parisi-Zhang equation is made and then used to discuss the scaling behavior and finite-size effects. Unfortunately it is difficult to make any direct numerical comparison between our results and those on coupled map lattices. Although the thrust of their investigation is very similar, the models are sufficiently different to preclude this, at least for the results presented here. Their models are purely one-dimensional coupled lattice models of size range 1000–8000, while ours are two-dimensional hard-disk systems, of at most 100 particles in a restricted geometry that makes them seem almost one dimensional. The fact that Refs. [19,20] can make a connection with the Kardar-Parisi-Zhang equation and then discuss the scaling behavior of finite-size effects is very appealing. For our system we are unable to perform simulations that are large enough to consider finite-size effects, but it is something that may be possible in the future.

Results in this paper suggest that the localized behavior of the Lyapunov vectors comes from the short range property of the particle interactions (Fig. 5), noting that the hard-core interaction of the systems used in this paper is the shortest range interactions possible. Therefore it should be interesting to compare our results with the Lyapunov localization of systems with longer range particle interactions. As mentioned in the Introduction of this paper, a conjecture about a relation between the Lyapunov localization and the existence of the thermodynamical limit of the largest Lyapunov exponent is suggested, however we have not explored this here. It seems plausible that Lyapunov localization may be a sufficient but not necessary condition for the existence of the thermodynamical limit for the largest Lyapunov exponent. This conjecture remains to be tested.

ACKNOWLEDGMENTS

One of the authors (T.T) wishes to thank T. Harayama and H. Schomerus for valuable information about localization problems. We are grateful to the Australian Research Council for financial support for this work.

APPENDIX A: INEQUALITY FOR THE LOCALIZATION WIDTH

In this appendix we derive inequality (10) for the localization width of the Lyapunov vector.

First we note the inequality $0\leqslant S^{(n)}$ which comes from Eqs. (5) and (8). This leads to the inequality $1\leqslant\mathcal{W}^{(n)}$.

Second, we note

$$\begin{aligned}
&\ln N+\sum_{j=1}^{N}\gamma_j^{(n)}(t)\ln\gamma_j^{(n)}(t)\\
&\quad=N^{-1}\sum_{j=1}^{N}[\gamma_j^{(n)}(t)N]\ln[\gamma_j^{(n)}(t)N]\\
&\quad=N^{-1}\sum_{j=1}^{N}\{[\gamma_j^{(n)}(t)N]\ln[\gamma_j^{(n)}(t)N]-[\gamma_j^{(n)}(t)N]+1\}\\
&\quad=N^{-1}\sum_{j=1}^{N}\mathcal{F}(\gamma_j^{(n)}(t)N),
\end{aligned}\tag{A1}$$

where we used Eq. (4), and the function $\mathcal{F}(x)$ of x is defined by

$$\mathcal{F}(x)\equiv x\ln x-x+1.\tag{A2}$$

It is easy to show that the function $\mathcal{F}(x)$ satisfies the inequality

$$\mathcal{F}(x)\geqslant 0\quad\text{in}\quad x\geqslant 0.\tag{A3}$$

Equations (8) and (A1), and inequality (A3) lead to

$$\ln N-S^{(n)}=N^{-1}\sum_{j=1}^{N}\langle\mathcal{F}(\gamma_j^{(n)}(t)N)\rangle\geqslant 0,\tag{A4}$$

noting the inequality $\gamma_j^{(n)}(t)N\geqslant 0$. Therefore we obtain the inequality $\mathcal{W}^{(n)}\leqslant N$ using Eq. (9). From the two inequalities $1\leqslant\mathcal{W}^{(n)}$ and $\mathcal{W}^{(n)}\leqslant N$ we derive the inequality (10) for the localization width.

We can also show that the function $\mathcal{F}(x)$ defined by Eq. (A2) satisfies $\mathcal{F}(x)=0$ only when $x=1$. Using this point and Eqs. (9) and (A4) we get the fact that the equality $\mathcal{W}^{(n)}=N$ for the localization width is satisfied only when all the quantities $\gamma_j^{(n)}(t)$, $j=1,2,\ldots N$ are equal, namely, when $\gamma_j^{(1)}(t)=\gamma_j^{(2)}(t)=\cdots=\gamma_j^{(N)}(t)=1/N$.

APPENDIX B: COMPARISON WITH SQUARE CASES

In this appendix we discuss differences between quasi-one-dimensional systems and square systems for the Lyapunov localization and its related phenomena. For the

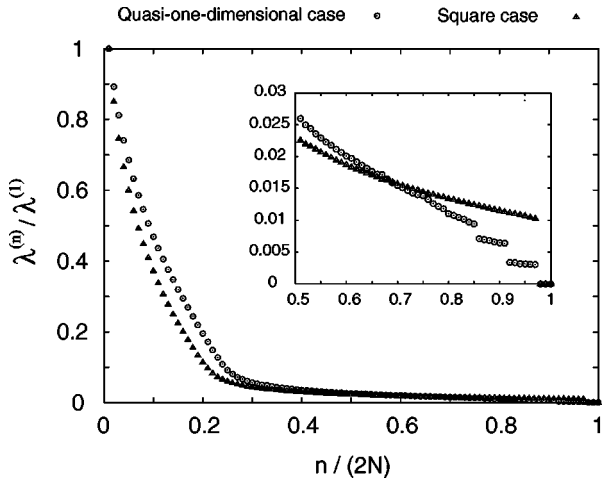

FIG. 17. The Lyapunov spectra normalized by the largest Lyapunov exponent $\lambda^{(1)}$ as functions of the normalized Lyapunov index $n/(2N)$ in the case of $d=10^5$ in the quasi-one-dimensional system (circles) and the square system (triangles). Inset: Enlarged graphs of the normalized Lyapunov spectra in a region of small positive Lyapunov exponents.

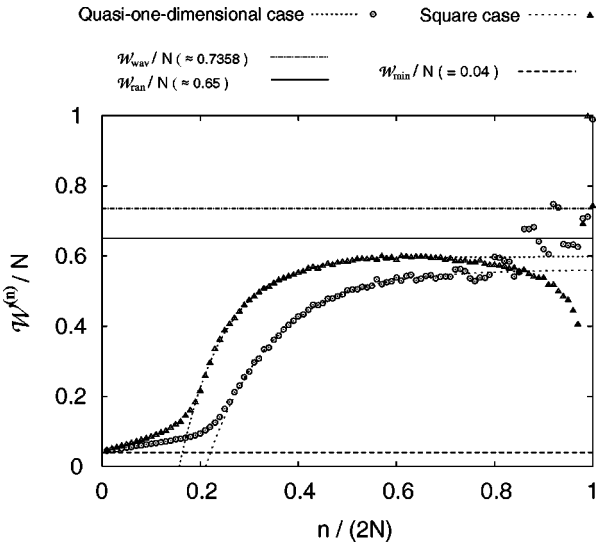

FIG. 18. Normalized localization width $\mathcal{W}^{(n)}/N$ as a function of the normalized Lyapunov index $n/(2N)$ in the case of $d=10^5$ in the quasi-one-dimensional case (circles) and the square case (triangles). The dotted lines are fits by exponential functions (the dependence $[\mathcal{E}D]$). The dash-dotted line, solid line, and dashed line correspond to $\mathcal{W}^{(n)}=\mathcal{W}_{wav}$ ($\approx 0.736N$), $\mathcal{W}_{ran}$ ($\approx 0.651N$), and $\mathcal{W}_{min}$ ($=2$), respectively.

quasi-one-dimensional system in this paper we choose the system lengths as

$$L_y = L_y' \equiv 2R(1+10^{-6}), \tag{B1}$$

$$L_x = L_x' \equiv NL_y(1+d)$$

$$[\text{in the quasi-one-dimensional cases}] \tag{B2}$$

with a parameter d to change the particle density. For meaningful comparisons between the square and quasi-one-dimensional cases we use system lengths for the square systems so that both cases give the same area, for the same value of the parameter d, namely,

$$L_y = L_x = \sqrt{L_x' L_y'} = \sqrt{N(1+d)[2R(1+10^{-6})]^2}$$

$$[\text{in the square cases}]. \tag{B3}$$

Except for these lengths L_x and L_y, we use the same parameter values as given in the text, such as $R=1$, $M=1$, and $E=N$. In this appendix we consider systems of 50 particles ($N=50$). In Appendixes B1, B2, B3, and B4 we consider the case of $d=10^5$ in which the linear dependence $[\mathcal{L}D]$ of localization widths with respect to Lyapunov index appears. In Appendix B 5 we discuss boundary effects in the localization width in the case of $d=0.5$.

1. Lyapunov spectra

The first example is the Lyapunov spectra of the quasi-one-dimensional case and the square case. Figure 17 is the positive branch of the normalized Lyapunov spectra as functions of the normalized Lyapunov index $n/(2N)$ in the quasi-one-dimensional system and the square system for $d=10^5$. Here the values of the largest Lyapunov exponents are given by $\lambda^{(1)}\approx 0.000\,157$ in the quasi-one-dimensional system, and $\lambda^{(1)}\approx 0.000\,552$ in the square system. As shown in Fig. 17, a sharp bending of the Lyapunov spectra occurs in both cases, but it occurs at a slightly smaller Lyapunov index in the square case than in the quasi-one-dimensional case. The Lyapunov spectrum in the quasi-one-dimensional case is also shown in Fig. 9.

There is a difference between the quasi-one-dimensional case and the square case in the region of small positive Lyapunov exponents. In the inset to Fig. 17, we can recognize two stepwise structures of the Lyapunov spectrum consisting of six Lyapunov exponents in the quasi-one-dimensional system. It should be noted that each of these steplike structures consists of one four-point step and one two-point step although these two steps are too close to be distinguished in Fig. 17. (This is also evidenced by investigating wavelike structures of the Lyapunov vectors, the so called Lyapunov modes [25].) On the other hand, we cannot recognize any stepwise structure in the square case, because 50 particles in a square system with density $\rho = 0.000\,007\,85\ldots$ is too small to show a stepwise structure of the Lyapunov spectrum. (It is known that rectangular systems including the quasi-one-dimensional systems show a longer stepwise region of Lyapunov spectra than in the square system with the same area [5].) In the square system the gap between the smallest nonzero positive Lyapunov exponent λ_{2N-4} and the zero Lyapunov exponents is larger than in the quasi-one-dimensional system.

2. Localization widths

Next we consider the localization width in the quasi-one-dimensional case and the square case in Fig. 18 for $d=10^5$. In the region of the Lyapunov index corresponding to the Lyapunov spectra changing smoothly, qualitative behav-

ior of the localization width are rather similar, and consist of the linear dependence $[\mathcal{L}D]$ in small Lyapunov indices and the exponential dependence $[\mathcal{E}D]$ in other indices, although the region of the linear dependence $[\mathcal{L}D]$ in the square case is slightly smaller than in the quasi-one-dimensional case. In Fig. 18 we give fits of exponential functions $y=\tilde{\alpha}+\tilde{\beta}\exp(\tilde{\gamma}x)$ for the exponential dependence $[\mathcal{E}D]$ by dotted lines. (The parameter values to fit data are $(\tilde{\alpha},\tilde{\beta},\tilde{\gamma})=(0.560\,814,-2.733\,48,-7.505\,44)$ for the quasi-one-dimensional case, and $(\tilde{\alpha},\tilde{\beta},\tilde{\gamma})=(0.597\,656,-3.353\,86,-10.9674)$ for the square case.) The localization widths are larger than their minimum value $\mathcal{W}^{(n)}=\mathcal{W}_{min}=2$ and are smaller than the random component case $\mathcal{W}^{(n)}=\mathcal{W}_{ran}\approx 0.651N$ except in the stepwise region of the Lyapunov spectra, and the smallest localization width $\mathcal{W}^{(1)}$ is close to $\mathcal{W}_{min}$ in both the cases.

As in the Lyapunov spectra, the localization width shows a different behavior with the Lyapunov index corresponding to the stepwise structure of the Lyapunov spectra. As we have already mentioned, in the square case of $N=50$ there is no stepwise region of the Lyapunov spectrum, so there is not a corresponding structure in the localization width. We can see that in the square case the localization widths $\mathcal{W}^{(n)}$ decrease as a function of the Lyapunov index n in the region of large Lyapunov indices corresponding to small positive Lyapunov exponents. On the other hand, we can see the effect of the stepwise structure of the Lyapunov spectrum on the localization width of the quasi-one-dimensional case. Especially a pair of two dots on the line $\mathcal{W}^{(n)}=\mathcal{W}_{wav}$ correspond to the two-point step of the Lyapunov spectrum shown in Fig. 17, supporting that in the Lyapunov spectrum of Fig. 17 for the quasi-one-dimensional case the first (second) step of the Lyapunov spectrum is a four-point step (a two-point step) looking from the zero-Lyapunov exponents.

3. Angle between the spatial and momentum parts of the Lyapunov vector

Figure 19 shows the time-averaged angles $\langle\theta^{(n)}\rangle/\pi$, $n=1,2,\ldots,2N$ between the spatial and momentum parts of the Lyapunov vectors for the quasi-one-dimensional and the square system as functions of the normalized Lyapunov index $n/(2N)$ for $d=10^5$. In both the cases, the angle $\theta^{(n)}$ is a rapidly increasing function of the Lyapunov index n in the linear dependence $[\mathcal{L}D]$ region of the localization width, and almost $\pi/2$ in the exponential dependence $[\mathcal{E}D]$ region.

We can see the stepwise structure in the angle $\theta^{(n)}$ as a function of the Lyapunov index n in the quasi-one-dimensional case (see the inset to Fig. 19). This structure corresponds to the stepwise structure of the Lyapunov spectrum shown in Fig. 17.

4. Amplitudes of the *x* and *y* components of the spatial and momentum parts of the Lyapunov vectors

As the next quantities to investigate the difference between the quasi-one-dimensional case and the square case, we consider the amplitudes of the x and y components of the spatial and momentum parts of the Lyapunov vectors. Figure

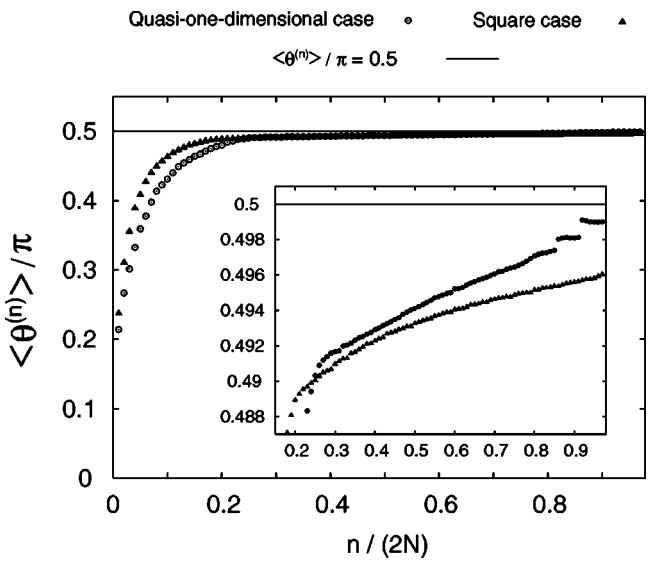

FIG. 19. The normalized time-average $\langle\theta^{(n)}\rangle/\pi$ of the angles between the spatial and momentum parts of the Lyapunov vectors in the quasi-one-dimensional case (circles) and the square case (triangles) as functions of the normalized Lyapunov index $n/(2N)$ for $d=10^5$. The solid line corresponds to the value $\theta^{(n)}=\pi/2$ of the angle. Inset: Enlarged graphs of normalized angles $\langle\theta^{(n)}\rangle/\pi$ in the region of Lyapunov index in which the exponential dependence $[\mathcal{E}D]$ of the localization widths (and the stepwise structure of the Lyapunov spectrum) appears.

20 shows the graphs of the time averages of normalized amplitudes of the x and y components of the spatial part and the momentum part of the Lyapunov vectors as functions of the normalized Lyapunov index $n/(2N)$ for the square with $d=10^5$. The corresponding graphs for the quasi-one-dimensional case are shown in Fig. 11(d). In the square system there is no difference between the x and y directions, so there is no gap between the x and y components in the spatial part and the momentum part of the Lyapunov vectors (except for those where the spatial part corresponds to the zero-Lyapunov exponents). Although the momentum parts $\langle\eta_{px}^{(n)}(t)\rangle$ and $\langle\eta_{py}^{(n)}(t)\rangle$ [the spatial parts $\langle\eta_{qx}^{(n)}(t)\rangle$ and $\langle\eta_{qy}^{(n)}(t)\rangle$] are rapidly decreasing (increasing) functions of the Lyapunov index in the region of the linear dependence $[\mathcal{L}D]$ of the localization widths (see the small figure on the top right of Fig. 20 for the momentum parts of the Lyapunov vectors. Also note the normalization condition (20) to know the corresponding spatial parts), the boundary of the two dependences $[\mathcal{L}D]$ and $[\mathcal{E}D]$ is not so clear in this figure.

In Fig. 20 we cannot recognize a stepwise structure of the quantities $\langle\eta_{qx}^{(n)}(t)\rangle$, $\langle\eta_{qy}^{(n)}(t)\rangle$, $\langle\eta_{px}^{(n)}(t)\rangle$, and $\langle\eta_{py}^{(n)}(t)\rangle$, because there is no stepwise structure of the Lyapunov spectrum in this system. It may be noted that the normalized x component $\langle\eta_{px}^{(n)}(t)\rangle$ and the normalized y component $\langle\eta_{py}^{(n)}(t)\rangle$ of the momentum part of the Lyapunov vectors corresponding to the zero Lyapunov exponents $\lambda^{(2N-2)}$, $\lambda^{(2N-1)}$, and $\lambda^{(2N)}$ are almost zero, as in the quasi-one-dimensional case.

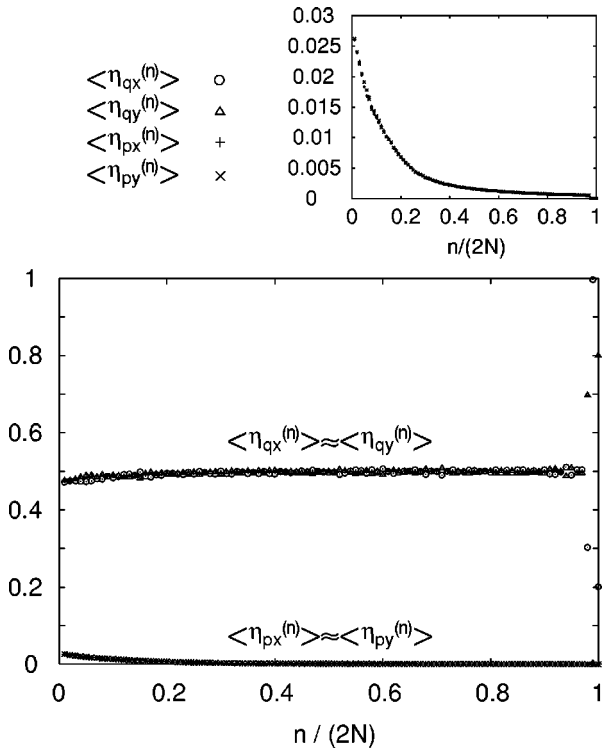

FIG. 20. Time average of the normalized amplitudes of the x component of the spatial part $[\langle \eta_{qx}^{(n)}(t)\rangle$, circles], the y component of the spatial part $[\langle \eta_{qy}^{(n)}(t)\rangle$, triangles], the x component of the momentum part $[\langle \eta_{px}^{(n)}(t)\rangle$, pluses], and the y component of the momentum part $[\langle \eta_{py}^{(n)}(t)\rangle$, crosses] of the Lyapunov vectors as functions of the normalized Lyapunov index $n/(2N)$ for a square system with $d=10^5$. The corresponding quasi-one-dimensional case is given in Fig. 11(d). The values of $\langle \eta_{qx}^{(n)}(t)\rangle$ and $\langle \eta_{qy}^{(n)}(t)\rangle$ are almost indistinguishable (except at the points corresponding to the zero Lyapunov exponents). Similarly, the values of $\langle \eta_{px}^{(n)}(t)\rangle$ and $\langle \eta_{py}^{(n)}(t)\rangle$ are indistinguishable. The small panels at the top right-hand side shows the graphs of $\langle \eta_{px}^{(n)}(t)\rangle$ and $\langle \eta_{py}^{(n)}(t)\rangle$ on a smaller scale showing again that these two properties are indistinguishable.

5. Boundary effects in the localization widths

As the last example in this appendix we check boundary effects in Lyapunov localizations. In this section we calculate the localization widths for square systems and quasi-one-dimensional systems with purely hard-wall boundary conditions or purely periodic boundary conditions. To give reasonable comparisons between the hard-wall boundary cases and the periodic boundary cases we choose the system lengths L_x and L_y so that the effective region for a particle to move is the same in both cases. This means that if we choose the system size as $L_x=\tilde{L}_x$ and $L_y=\tilde{L}_y$ for the periodic boundary case, then they must be $L_x=\tilde{L}_x+2R$ and $L_y=\tilde{L}_y+2R$ for the corresponding hard-wall boundary case. Except for this point, we choose the same value of the other parameters for these two boundary cases. In this section we use the value $d=0.5$. Note that in this case the linear dependence $[\mathcal{L}D]$ of the localization widths does not appear.

Figure 21 is a comparison of the normalized localization widths $\mathcal{W}^{(n)}/N$, $n=1,2,\ldots,2N$ for the square system with periodic boundary conditions, and hard-wall boundary conditions, and the quasi-one-dimensional system with periodic boundary conditions, and hard-wall boundary conditions. Figure 21 shows that the localization widths for hard-wall boundary conditions are smaller than for periodic boundary conditions in both square and quasi-one-dimensional systems. However it should be noted that differences in the values of the localization widths are rather small in the region of small Lyapunov indices n in which the Lyapunov vectors are strongly localized. This is a natural result because the Lyapunov localization is a local behavior so that it should not depend strongly on global conditions such as boundary conditions. We note that in very narrow systems, such as the quasi-one-dimensional system, a strong boundary effect appears because particles can collide with walls much more often than in square cases, and this could be the reason for the differences in the values of the localization widths for the different boundary conditions are larger in the quasi-one-dimensional system than in the square system. A part of the localization widths as a function of the Lyapunov index are nicely fitted by the exponential function $y=\tilde{\alpha}+\tilde{\beta}\exp(\tilde{\gamma}x)$ for the exponential dependence $[\mathcal{E}D]$ with fitting parameters $\tilde{\alpha}$, $\tilde{\beta}$ and $\tilde{\gamma}$, shown as the dotted lines in Fig. 21. Here, the values of fitting parameters are chosen as $(\tilde{\alpha},\tilde{\beta},\tilde{\gamma})=(0.653\,629,-0.377\,495,-10.9742$ for the square case with the periodic boundary conditions, $(\tilde{\alpha},\tilde{\beta},\tilde{\gamma})=(0.638\,696,-0.422\,529,-10.3554)$ for the square case with the

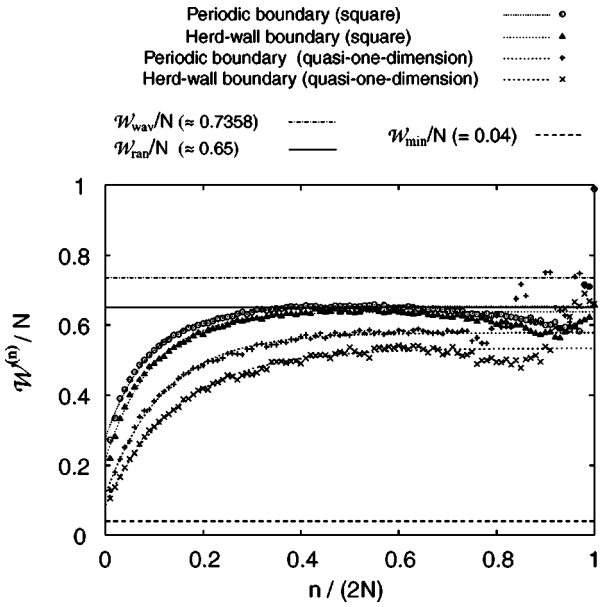

FIG. 21. Normalized localization widths $\mathcal{W}^{(n)}/N$ as functions of the normalized Lyapunov index $n/(2N)$ for $d=0.5$ in a square system with periodic boundary conditions (circles), in a square system with hard-wall boundary conditions (triangles), in a quasi-one-dimensional system with periodic boundary conditions (pluses), in a quasi-one-dimensional system with hard-wall boundary conditions (crosses). The dotted lines are fits of the numerical data by exponential functions. The dash-dotted line, solid line, and dashed line correspond to $\mathcal{W}^{(n)}=\mathcal{W}_{wav}$ $(\approx 0.736N)$, $\mathcal{W}_{ran}$ $(\approx 0.651N)$, and $\mathcal{W}_{min}$ $(=2)$, respectively.

hard-wall boundary conditions, $(\tilde{\alpha},\tilde{\beta},\tilde{\gamma})=(0.578\,304, -0.464\,099, -8.414\,39)$ for the quasi-one-dimensional periodic boundary case, and $(\tilde{\alpha},\tilde{\beta},\tilde{\gamma})=(0.534\,472, -0.449\,403, -6.762\,48)$ for the quasi-one-dimensional hard-wall boundary case. It may also be noted that the part of the localization widths corresponding to the Lyapunov spectrum changing smoothly seems to be slightly larger than the value $\mathcal{W}_{ran}$ for the localization width for random components in the square system with periodic boundary conditions and $d=0.5$ in Fig. 21.

In the quasi-one-dimensional periodic boundary case in Fig. 21 we can recognize two pairs of localization widths on the line $\mathcal{W}^{(n)}=\mathcal{W}_{wav}$ corresponding to the two-point steps of the Lyapunov spectra, but there is not a localization width of this value in the hard-wall boundary case. This comes from the fact that in the periodic boundary case the system satisfies total momentum conservation leading to the two-point steps of the Lyapunov spectrum whereas the system with hard-wall boundary conditions does not satisfy such a conservation in any direction (details of this point were discussed in Ref. [25]).

[1] P. Gaspard, *Chaos, Scattering and Statistical Mechanics* (Cambridge University Press, Cambridge, 1998).

[2] I. Goldhirsh, P.-L. Sulem, and S.A. Orszag, Physica D **27**, 311 (1987).

[3] K. Ikeda and K. Matsumoto, J. Stat. Phys. **44**, 955 (1986).

[4] T. Konishi and K. Kaneko, J. Phys. A **25**, 6283 (1992).

[5] H.A. Posch and R. Hirschl, in *Hard Ball Systems and the Lorentz Gas*, edited by D. Szász (Springer, Berlin, 2000), p. 279.

[6] J.-P. Eckmann and O. Gat, J. Stat. Phys. **98**, 775 (2000).

[7] S. McNamara and M. Mareschal, Phys. Rev. E **64**, 051103 (2001).

[8] T. Taniguchi and G.P. Morriss, Phys. Rev. E **65**, 056202 (2002).

[9] P. Manneville, Lect. Notes Phys. **230**, 319 (1985).

[10] K. Kaneko, Physica D **23**, 436 (1986).

[11] G. Giacomelli and A. Politi, Europhys. Lett. **15**, 387 (1991).

[12] H. Chaté, Europhys. Lett. **21**, 419 (1993).

[13] R. Livi and S. Ruffo, in *Nonlinear Dynamics*, edited by G. Turchetti (World Scientific, Singapore, 1989), p. 220.

[14] M. Falcioni, U.M.B. Marconi, and A. Vulpiani, Phys. Rev. A **44**, 2263 (1991).

[15] Lj. Milanović and H.A. Posch, J. Mol. Liq. **96-97**, 221 (2002).

[16] C. Forster, R. Hirschl, H.A. Posch, and W.G. Hoover, Physica D (to be published), e-print nlin.CD/0211047.

[17] S. Lepri, A. Politi, and A. Torcini, J. Stat. Phys. **82**, 1429 (1996).

[18] I.M. Lifshits, S.A. Gredeskul, and L.A. Pastur, *Introduction to the Theory of Disordered Systems*, translated from the Russian by E. Yankovsky (Wiley-Interscience, New York, 1988).

[19] A.S. Pikovsky and J. Kurths, Phys. Rev. E **49**, 898 (1994).

[20] A. Pikovsky and A. Politi, Nonlinearity **11**, 1049 (1998).

[21] A. Pikovsky and A. Politi, Phys. Rev. E **63**, 036207 (2001).

[22] R. Livi, A. Politi, S. Ruffo, and A. Vulpiani, J. Stat. Phys. **46**, 147 (1987).

[23] Ya.G. Sinai, Int. J. Bifurcation Chaos Appl. Sci. Eng. **6**, 1137 (1996).

[24] T. Taniguchi, C.P. Dettmann, and G.P. Morriss, J. Stat. Phys. **109**, 747 (2002).

[25] T. Taniguchi and G. P. Morriss, Phys. Rev. E **68**, 026218 (2003).

[26] The density ρ used in this paper is the reduced density, and is defined as the ratio of the area $(N\pi R^2)$ occupied by hard disks to the total area (L_xL_y). This should be distinguished from another density called the particle number density which is defined by $\tilde{\rho}\equiv N(2R)^2/L_xL_y$ in our notation. The particle number density has been used in some works using many-hard-disk systems with $R=1/2$ [15,16]. These two kinds of density are simply related by $\rho=\pi\tilde{\rho}/4$.

[27] G. Benettin, L. Galgani, and J.-M. Strelcyn, Phys. Rev. A **14**, 2338 (1976).

[28] I. Shimada and T. Nagashima, Prog. Theor. Phys. **61**, 1605 (1979).

[29] G. Benettin, L. Galgani, A. Giorgilli, and J.-M. Strelcyn, Meccanica **15**, 9 (1980).

[30] G. Benettin, L. Galgani, A. Giorgilli, and J.-M. Strelcyn, Meccanica **15**, 21 (1980).

[31] Ch. Dellago, H.A. Posch, and W.G. Hoover, Phys. Rev. E **53**, 1485 (1996).

[32] There may be exceptional cases in which localization widths $\mathcal{W}^{(n)}$ in the Lyapunov index corresponding to the continuous part of the Lyapunov spectrum are larger than $\mathcal{W}_{ran}$ in very high density cases. See the graph of localization widths for the square system in Appendix B 5.

[33] See Fig. 10 in Ref. [40]. Note that in this figure the Lyapunov exponents are plotted by a logarithmic scale, in which the sharp bend of the Lyapunov spectrum is represented as a mild step of the Lyapunov spectrum.

[34] R. Livi, M. Pettini, S. Ruffo, and A. Vulpiani, J. Stat. Phys. **48**, 539 (1987).

[35] Y.Y. Yamaguchi, J. Phys. A **31**, 195 (1998).

[36] H. van Beijeren, A. Latz, and J.R. Dorfman, Phys. Rev. E **57**, 4077 (1998).

[37] R. van Zon, H. van Beijeren, and Ch. Dellago, Phys. Rev. Lett. **80**, 2035 (1998).

[38] P. Collet and J.-P. Eckmenn, e-print nlin.CD/0303002.

[39] Ch. Dellago and H.A. Posch, Phys. Rev. E **55**, R9 (1997).

[40] P. Gaspard and H. van Beijeren, J. Stat. Phys. **109**, 671 (2002).

[41] N.S. Krylov, *Works on the Foundations of Statistical Physics*, A.B. Migdal, Ya. G. Sinai, and Yu. L. Zeeman, Princeton Series in Physics (Princeton University Press, Princeton, NJ, 1979).

[42] Ch. Dellago and H.A. Posch, Physica A **240**, 68 (1997).

[43] H. van Beijeren and J.R. Dorfman, Phys. Rev. Lett. **74**, 4412 (1995).

[44] N. Chernov, J. Stat. Phys. **88**, 1 (1997).

[45] M. Cencini, M. Falcioni, E. Olbrich, H. Kantz, and A. Vulpiani, Phys. Rev. E **62**, 427 (2000).

[46] G. Boffetta, M. Cencini, M. Falcioni, and A. Vulpiani Phys. Rep. **356**, 367 (2002).

[47] G. Casati and T. Prosen, Phys. Rev. Lett. **83**, 4729 (1999).

[48] C.P. Dettmann, E.G.D. Cohen, and H. van Beijeren, Nature (London) **401**, 875 (1999).
[49] C. Dettmann and E.G.D. Cohen, J. Stat. Phys. **101**, 775 (2000).
[50] C. Dettmann and E.G.D. Cohen, J. Stat. Phys. **103**, 589 (2001).
[51] F. Cecconi, D. del-Castillo-Negrete, M. Falcioni, and A. Vulpiani, Physica D **180**, 129 (2003).
[52] B. Li, G. Casati, and J. Wang, Phys. Rev. E **67**, 021204 (2003).
[53] S. Lepri, L. Rondoni, and G. Benettin, J. Stat. Phys. **99**, 857 (2000).
[54] J.R. Dorfman, *An Introduction to Chaos in Nonequilibrium Statistical Mechanics* (Cambridge University Press, Cambridge, 1999).